Modified Gravity or Dark Energy

as the Drivers of the Late-Time Acceleration of the Universe?

Geometric Foundations of Gravity 2026 (Tartu, Estonia)

Mariam Bouhmadi-López

IKERBASQUE & EHU (Spain)

June 29th, 2026

Table of contents

Introduction

Introduction-1-: A brief sketch of the universe

- The universe is homogeneous and isotropic on large scales (cosmological principle)
- The matter content of the universe:
  - Standard matter
  - Dark matter
  - Something that induce the late-time acceleration of the Universe
- The acceleration of the universe is backed by several measurments: $H(z)$, Snela, BAO, CMB, LSS (matter power spectrum, growth function)...

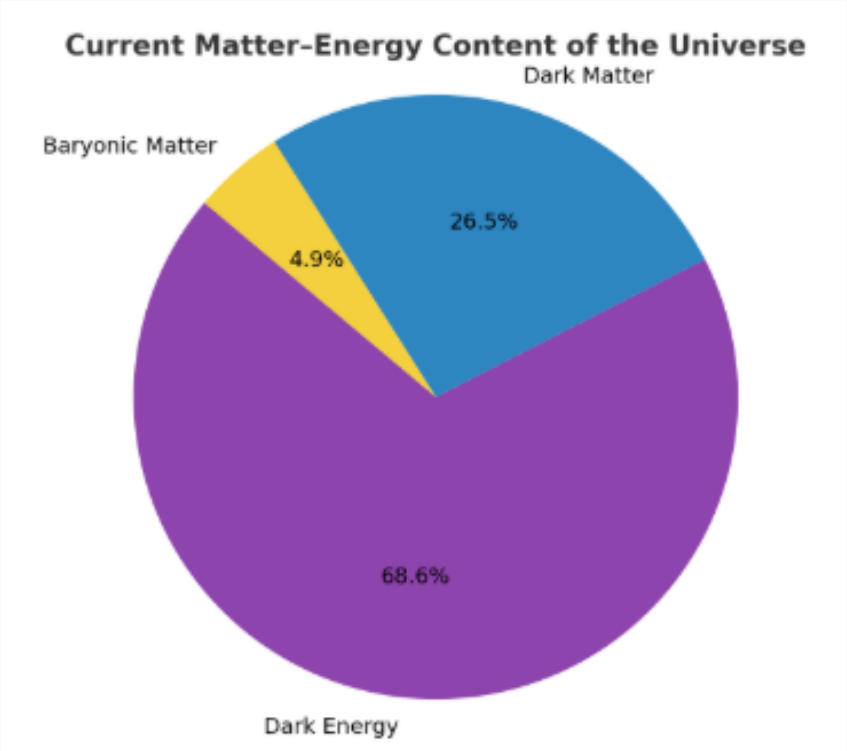

Introduction-2-

- The effective equation of state of whatever is driving the current speed up of the universe is roughly -1.
- Such an acceleration could be due to:
  - A new component of the energy budget of the universe: dark energy; i.e. it could be Λ (i.e. a non dynamical dark energy), quintessence, of a phantom(-like/effective) nature
  - A change on the behaviour of gravity on the largest scale. No new component on the budget of the universe but rather simply gravity modifies its behaviour, within a metric, Palatini (affine metric), in presence of torsion or non-metricity ....

Cosmological problems

- If Λ is driving the current acceleration of the Universe, then:
  - Coincidence problem. How is this sensible to initial conditions?
  - Why now? Dark energy seems to be dominant only at late-time, not before.
  - Fine-tuning problem. New energetic scale $\rho_\Lambda \approx 10^{-47}\ \text{GeV}^4$. It is very small compared to other scales.
  - Cosmological tensions, in particular the Hubble tension.

Hubble tension

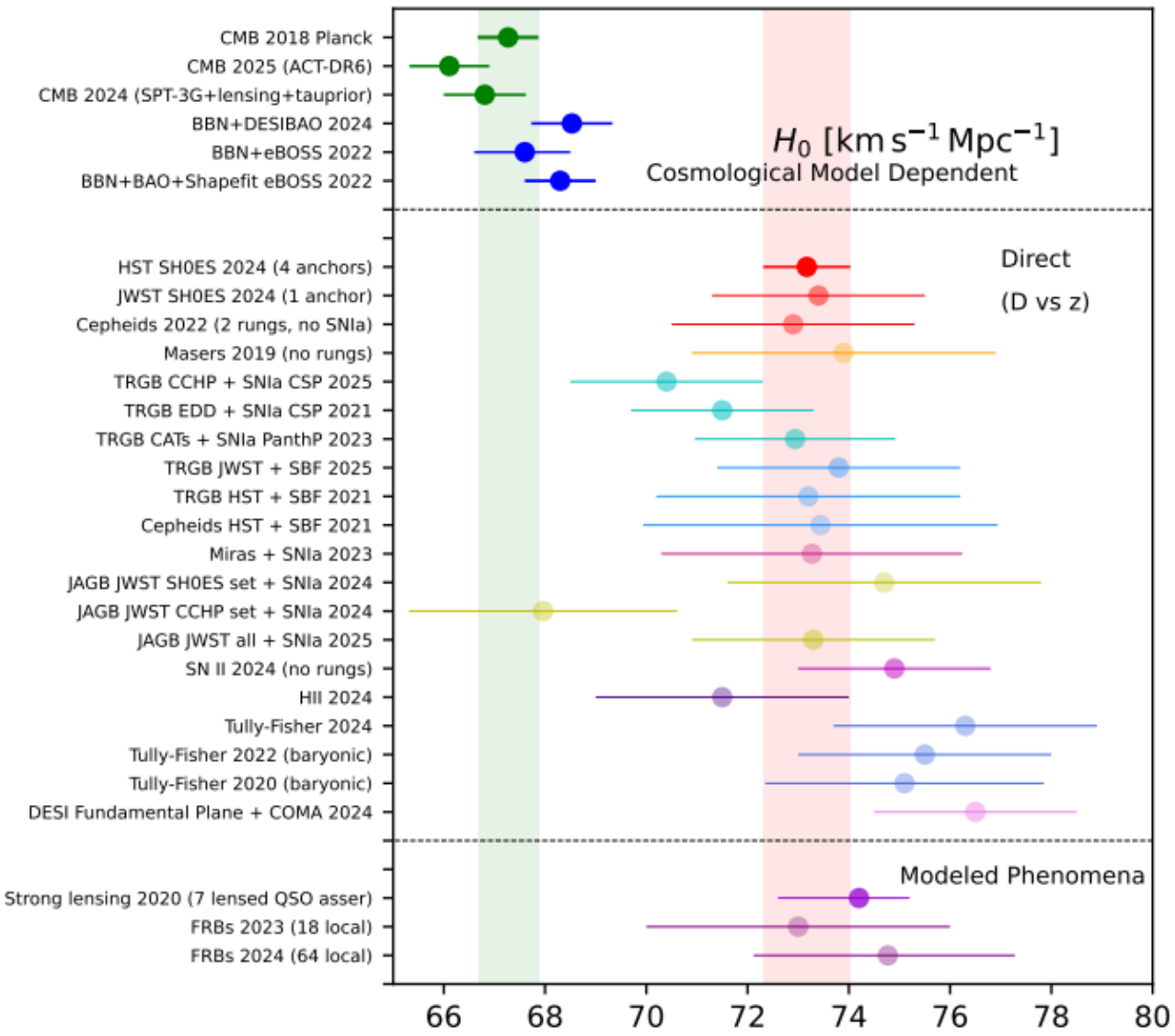

E. Di Valentino et al. [arXiv:2504.01669 [astro-ph.CO]]

S_8 tension

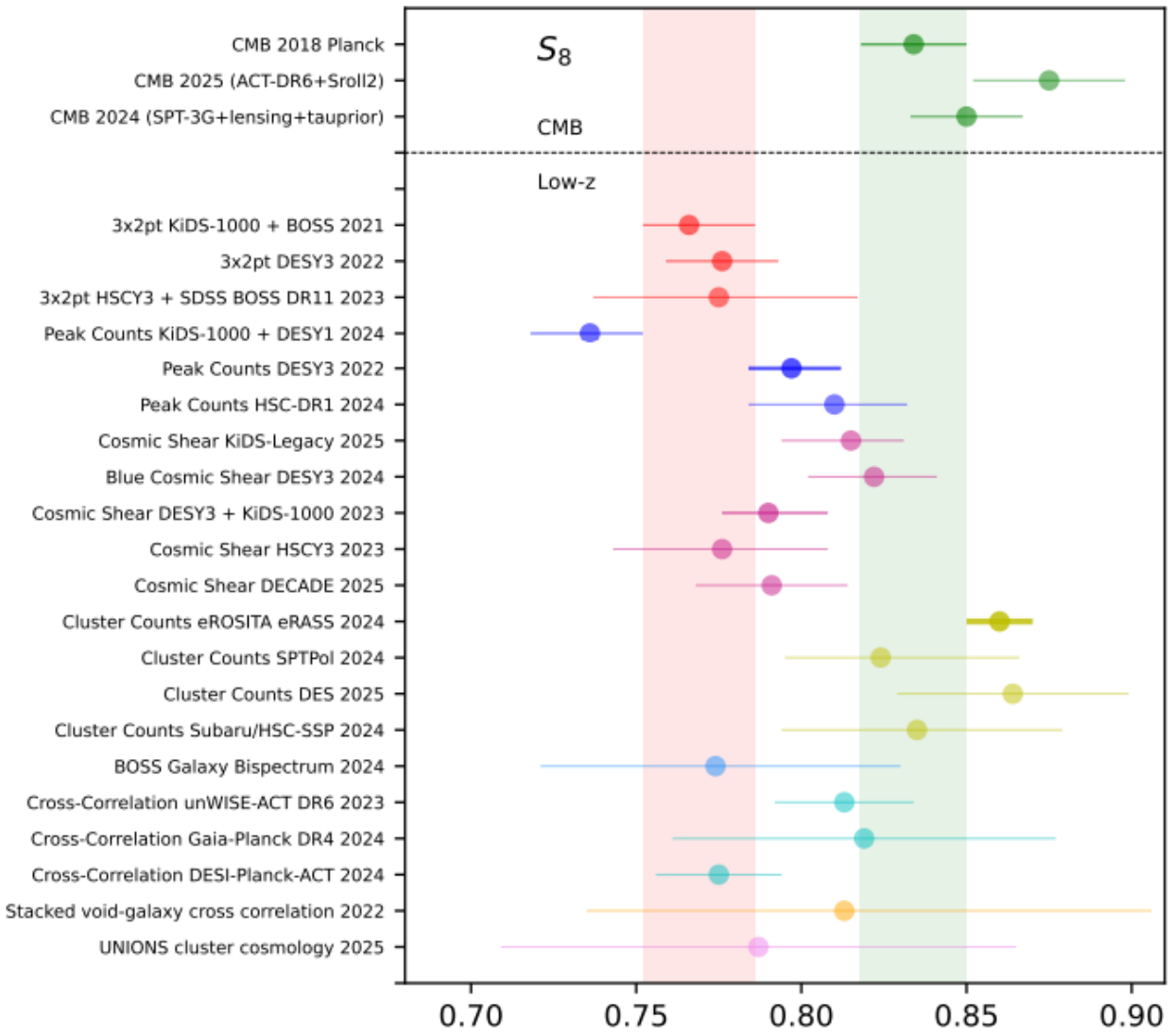

E. Di Valentino et al. [arXiv:2504.01669 [astro-ph.CO]]

In what ways could evolving dark energy models or extended theories of gravity help to resolve the issues outlined above?

Modified theory within $f(Q)$ gravity

Geometry of Spacetime: Metricity vs Non-Metricity

- We assume a space-time endowed with a metric $g_{\mu\nu}$ and a symmetric connection $\Gamma^{\lambda}_{\mu\nu}$, i.e. NO torsion:
- What is metricity, and how does it differ from non-metricity?

Metric Compatibility

$$\nabla_\lambda g_{\mu\nu} = 0$$

The covariant derivative of the metric tensor vanishes, meaning the length of vectors is preserved under parallel transport. Then the connection is uniquely determined by the metric and is given by the Levi-Civita connection.

Non-Metricity Tensor

$$Q_{\lambda\mu\nu} = \nabla_\lambda g_{\mu\nu} \neq 0$$

Represents the failure of the connection to preserve the metric under parallel transport. Therefore, the lenght of a vector may change.

J. M. Nester and H.-J. Yo, 1999

Curvature of Spacetime: Metricity vs Non-Metricity

- The scalar curvature of a space-time endowed with a metric $g_{\mu\nu}$ and a symmetric connection $\Gamma^{\lambda}_{\mu\nu}$ can be written as:

$$R(\Gamma) = \mathcal{R}(\{\}) + \mathrm{Q} + \text{surface terms},$$

where

$$Q := -\tfrac{1}{4} Q_{\alpha\mu\nu} Q^{\alpha\mu\nu} + \tfrac{1}{2} Q_{\alpha\mu\nu} Q^{\mu\alpha\nu} + \tfrac{1}{4} Q_{\alpha} Q^{\alpha} - \tfrac{1}{2} Q_{\alpha} \tilde{Q}^{\alpha}$$
$$Q_{\alpha} := Q_{\alpha\mu}{}^{\mu} \qquad \tilde{Q}_{\alpha} := Q_{\mu\alpha}{}^{\mu} \, .$$

- For a vanishing $R(\Gamma)$ a theory with Lagrangian density linear on $\mathcal{R}(\{\})$, is equivalent to a theory with Lagrangian density linear in Q.
- The former statment does not apply to $f(\mathcal{R}(\{\}))$ and $f(\mathrm{Q})$ because of the surface term.
- This gives rise to $f(\mathrm{Q})$ gravity as a new avenue of exploration, particularly from a phenomenological perspective, for example.

J. Beltrán Jiménez, L. Heisenberg, and T. S. Koivisto, arXiv:1803.10185 (JCAP)

$f(Q)$ gravity

- The gravitational action:

$$S = \int d^4x\sqrt{-g}\left[-\frac{1}{2}f(Q) + \mathcal{L}_M\right].$$

- The equations of motion are deduced by varying the action with respect to the metric and the connection.
- The energy momentum tensor for matter is conserved.

J. Beltrán Jiménez, L. Heisenberg, and T. S. Koivisto, arXiv:1803.10185 (proposer of the theories) (JCAP)

R. Lazkoz, F. S. N. Lobo, M. Ortiz-Baños, and V. Salzano, arXiv:1907.13219 (among the first cosmological fits) (PRD)

FLRW cosmology in $f(\mathbb{Q})$ gravity

- The metric:

$$\mathrm{d}s^2 = -N(t)\mathrm{d}t^2 + a^2(t)\left[\mathrm{d}r^2 + r^2\left(\mathrm{d}\theta^2 + \sin^2\theta\mathrm{d}\phi^2\right)\right] \ ,$$

- The connection must be consistent with the symmetries of the FLRW metric; it should also be symmetric and satisfy the flatness condition, i.e. $R(\Gamma) = 0$.
- There are three possible connections that satisfy the above criteria, highlighting the richness of the theory.
- From now on, we shall adopt the simplest choice for the connection, maintaining the FLRW metric in its standard form.

M. Hohmann, arXiv: 1912.12906 (Symmetry), F. D'Ambrosio, L. Heisenberg, and S. Kuhn, arXiv:2109.04209 (CQG), I. Ayuso, M. B.-L., C.-Y. Chen, X. Y. Chew, K. Dialektopoulos, Y. C. Ong, arXiv:2506.03506 (JCAP)

Suitable $f(\mathrm{Q})$ models for cosmology-1-

- Friedmann and Raychauduri equations:

$$6f_Q H^2 - \frac{1}{2}f = \rho_m \qquad \left(12H^2 f_{QQ} + f_Q\right)\dot{H} = -\frac{1}{2}(\rho_m + p_m)\,.$$

- The conservation equation:

$$\dot{\rho}_m + 3H(\rho_m + p_m) = 0.$$

- Three potential candidates:

$$\begin{aligned} f_1(Q) &= Q\exp\left(\lambda Q_0/Q\right), \\ f_2(Q) &= Q + Q_0\exp\left(-\lambda Q_0/Q\right), \\ f_3(Q) &= Q + \lambda Q_0[1-\exp\left(-Q_0/Q\right)]. \end{aligned}$$

- All these models give rise to late-time acceleration.
- The first model previously analysed in F. K. Anagnostopoulos, S. Basilakos and E. N.Saridakis, arXiv:2104.15123 [gr-qc] (PLB).

C.G. Boiza, M. Petronikolou, M.B.-L. and E. N. Saridakis: arXiv:2505.18264 (JCAP)

Suitable $f(\mathrm{Q})$ models for cosmology-2-

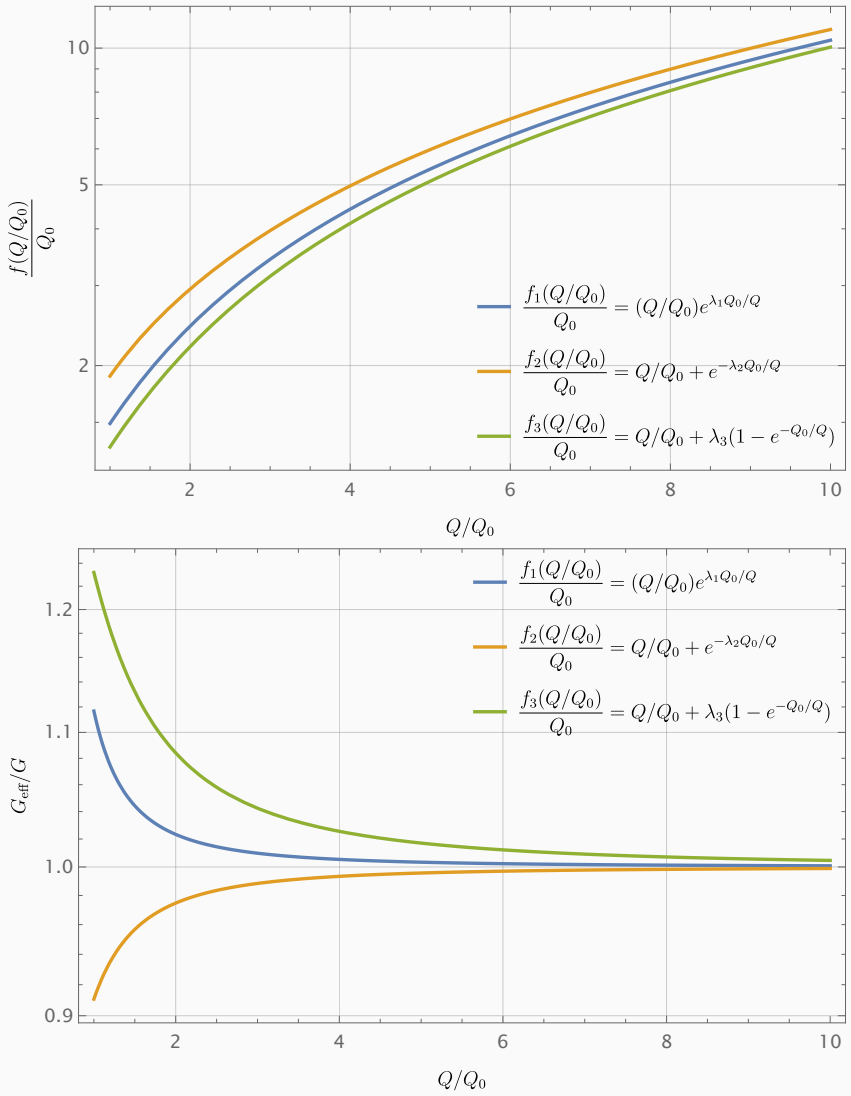

C.G. Boiza, M. Petronikolou, M.B.-L, E. N. Saridakis, arXiv:2505.18264 (JCAP)

Suitable $f(\mathrm{Q})$ models for cosmology-3-

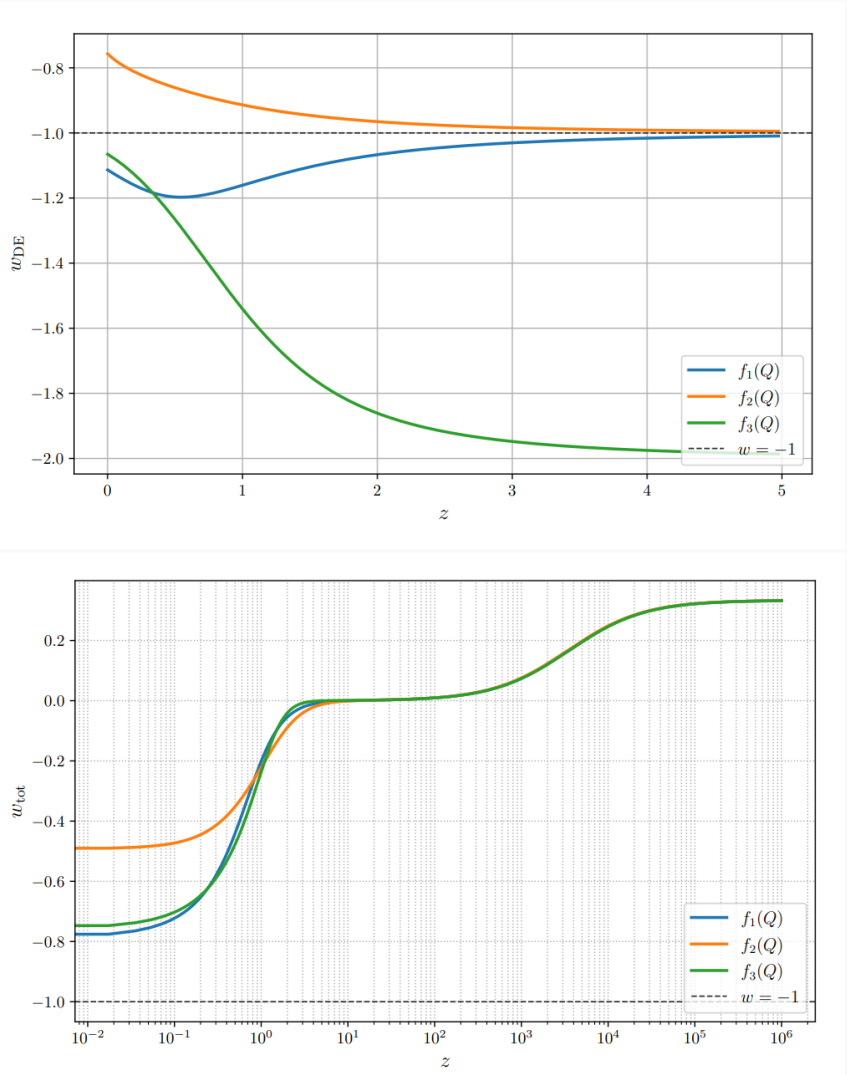

C.G. Boiza, M. Petronikolou, M.B.-L, E. N. Saridakis, arXiv:2505.18264 ((JCAP))

Observational constraints

- The analysis is performed for five different combinations of datasets:
  - **Combination I:** Cosmic chronometers (CC), supernovae (SN), and gamma-ray bursts (GRB);
  - **Combination II:** Baryon acoustic oscillations (BAO);
  - **Combination III:** Cosmic microwave background (CMB);
  - **Combination IV:** Baryon acoustic oscillations and cosmic microwave background (BAO + CMB);
  - **Combination V:** Full combination (CC + SN + GRB + BAO + CMB).

Fitting the model-1-

Model	H_0	Ω_{m0}	Ω_{b0}	ΔAIC
		CC + SN + GRB		
ΛCDM	68.67 ± 1.80	0.3037 ± 0.0202	–	–
$f_1(Q)$	68.56 ± 1.90	0.3489 ± 0.0206	–	0.192
$f_2(Q)$	69.34 ± 1.82	0.2608 ± 0.0159	–	1.65
$f_3(Q)$	68.70 ± 1.87	0.3524 ± 0.0226		0.227
		BAO		
ΛCDM	73.2 ± 15.0	0.2948 ± 0.0141	0.0545 ± 0.0160	–
$f_1(Q)$	74.4 ± 14.7	0.2897 ± 0.0138	0.0462 ± 0.0148	2.07
$f_2(Q)$	70.6 ± 14.9	0.3036 ± 0.0171	0.0617 ± 0.0180	0.454
$f_3(Q)$	73.6 ± 13.8	0.3065 ± 0.0140	0.0447 ± 0.0130	1.36
		CMB		
ΛCDM	67.273 ± 0.633	0.31649 ± 0.00867	0.049374 ± 0.000692	–
$f_1(Q)$	71.821 ± 0.709	0.27794 ± 0.00785	0.043329 ± 0.000664	0.00249
$f_2(Q)$	62.664 ± 0.622	0.36418 ± 0.00982	0.057004 ± 0.000910	-0.00365
$f_3(Q)$	73.579 ± 0.620	0.26422 ± 0.00641	0.041322 ± 0.000536	-0.000683
		BAO + CMB		
ΛCDM	66.910 ± 0.405	0.32157 ± 0.00562	0.049831 ± 0.000467	–
$f_1(Q)$	70.654 ± 0.451	0.29129 ± 0.00526	0.044473 ± 0.000452	3.74
$f_2(Q)$	62.746 ± 0.464	0.36277 ± 0.00730	0.056875 ± 0.000709	6.01
$f_3(Q)$	71.467 ± 0.464	0.28749 ± 0.00534	0.043213 ± 0.000438	16.0
		CC + SN + GRB + BAO + CMB		
ΛCDM	67.022 ± 0.377	0.32001 ± 0.00523	0.049719 ± 0.000443	–
$f_1(Q)$	70.431 ± 0.460	0.29392 ± 0.00543	0.044673 ± 0.000465	11.0
$f_2(Q)$	63.621 ± 0.419	0.34929 ± 0.00627	0.055671 ± 0.000603	37.1
$f_3(Q)$	70.942 ± 0.254	0.29362 ± 0.00295	0.043691 ± 0.000285	23.2

TABLE III: Mean values and standard deviations of the cosmological parameters obtained for each $f(Q)$ model, namely $f_1(Q) = Qe^{\lambda_1 Q_0/Q}$, $f_2(Q) = Q + Q_0 e^{-\lambda_2 Q_0/Q}$, and $f_3(Q) = Q + \lambda_3 Q_0\left[1 - e^{-Q_0/Q}\right]$, and for ΛCDM paradigm, under the five different dataset combinations considered in this work: **Combination I** (CC + SN + GRB), **Combination II** (BAO), **Combination III** (CMB), **Combination IV** (BAO + CMB), and **Combination V** (CC + SN + GRB + BAO + CMB). The last column shows the AIC difference, $\Delta\text{AIC} \equiv \text{AIC}_{f(Q)} - \text{AIC}_{\Lambda\text{CDM}}$, quantifying the statistical preference relative to the ΛCDM model.

C.G. Boiza, M. Petronikolou, M.B.-L. and E. N. Saridakis: arXiv:2505.18264 (JCAP)

Fitting the model-2-

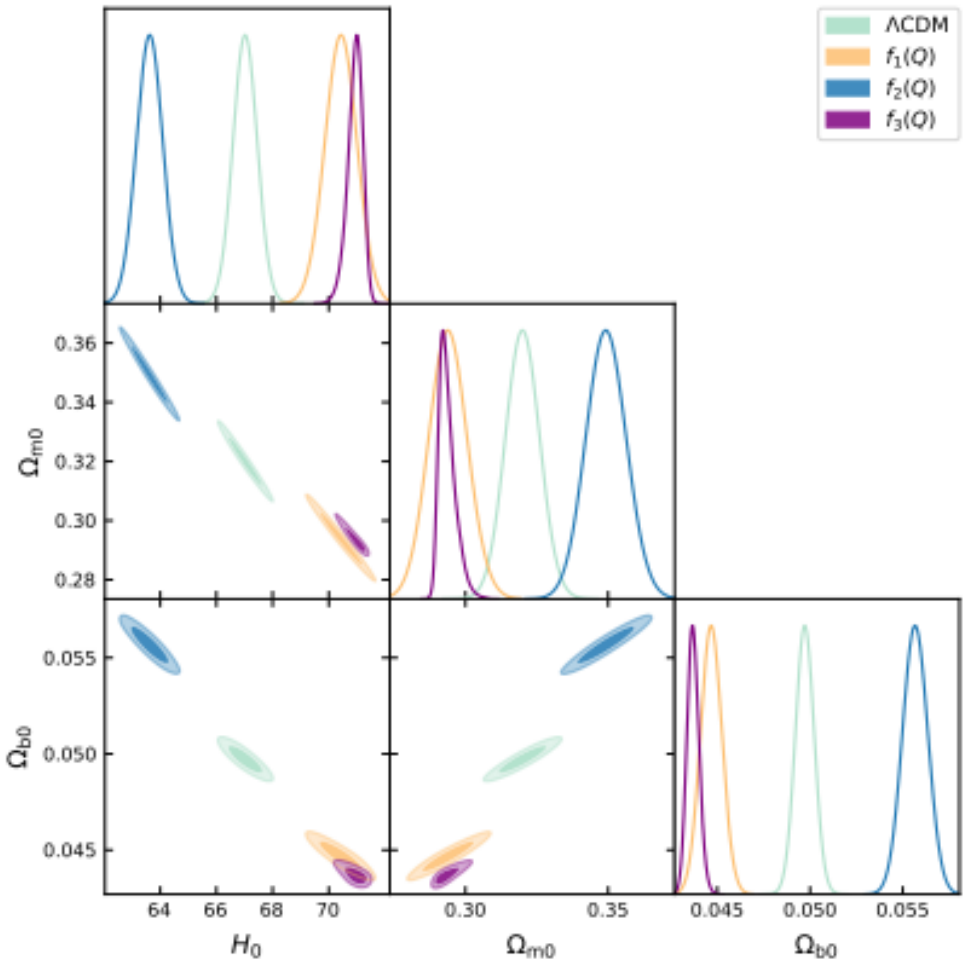

FIG. 2: *Two-dimensional posterior distributions for the $f(Q)$ models and ΛCDM scenario, using Combination V (CC + SN + GRB + BAO + CMB). The contours correspond to the 68% and 95% confidence levels (C.L.). This figure summarises the full parameter constraints, including Ω_{b0}. It illustrates how Models 1 and 3 accommodate higher values of H_0 in contrast to Model 2, which yields a lower H_0 compared to ΛCDM.*

Fitting the model-3-

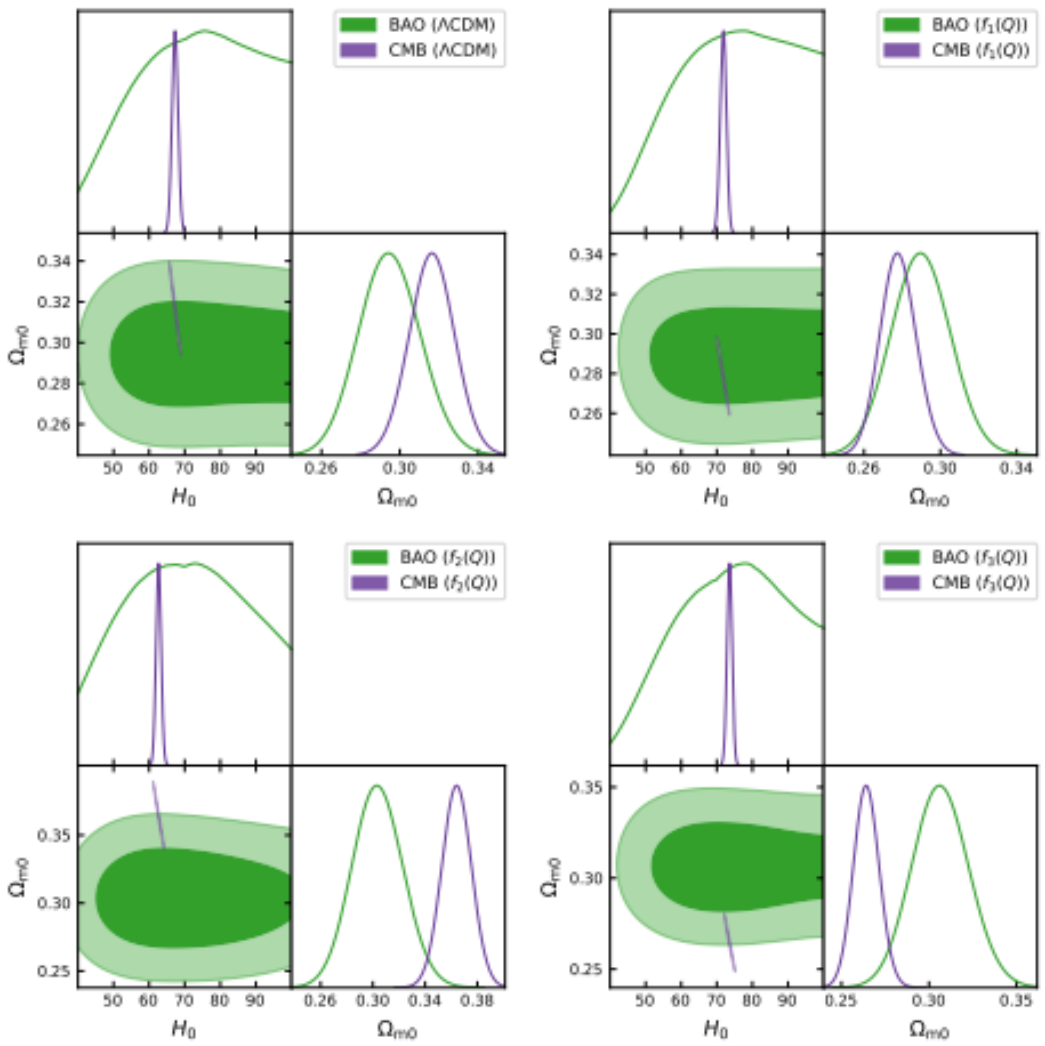

FIG. 4: *Comparison of the two-dimensional posterior distributions obtained from Combination II (BAO) and Combination III (CMB) for each model separately. The contours correspond to the 68% and 95% confidence levels (C.L.). The top-left panel shows the results for ΛCDM scenario, which displays excellent agreement between BAO and CMB. The remaining panels correspond to Models 1 (top-right), 2 (bottom-left), and 3 (bottom-right). A clear tension between BAO and CMB in the $\Omega_{m0} - H_0$ plane appears in Models 2 and 3.*

Fitting the model-4-

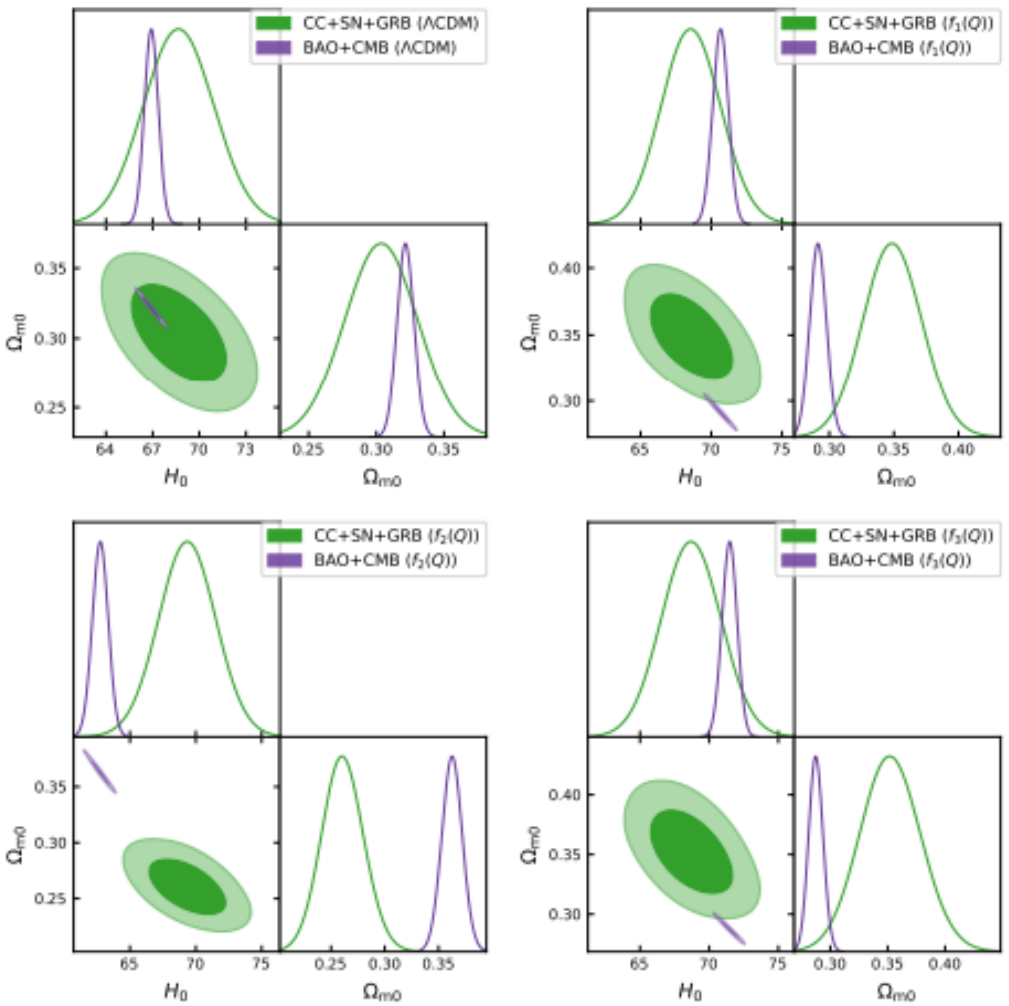

FIG. 5: *Comparison of the two-dimensional posterior distributions obtained from Combination I (CC + SN + GRB) and Combination IV (BAO + CMB) for each model separately. The contours correspond to the 68% and 95% confidence levels (C.L.). The top-left panel shows the results for ΛCDM scenario, which displays excellent agreement between the dataset combinations. The remaining panels correspond to Models 1 (top-right), 2 (bottom-left), and 3 (bottom-right), where a clear tension between the combinations emerges in the $\Omega_{m0} - H_0$ plane. These internal inconsistencies contribute to the poorer global fits obtained by the $f(Q)$ models when all datasets are combined.*

Modified theory within $f(T)$ gravity

Geometry of Spacetime: Torsion-Free vs Torsion

- We assume a space-time endowed with a metric $g_{\mu\nu}$ and a metric-compatible connection $\Gamma^{\lambda}_{\mu\nu}$, i.e. NO non-metricity:

$$\nabla_{\lambda} g_{\mu\nu} = 0.$$

- What is torsion, and how does it differ from a torsion-free geometry?

Torsion-Free Geometry

$$T^{\lambda}_{\mu\nu} = 0$$

The affine connection is symmetric, $\Gamma^{\lambda}_{\mu\nu} = \Gamma^{\lambda}_{\nu\mu}$. As a consequence, spacetime possesses no torsion. This is the case in General Relativity, where gravity is entirely described by the curvature of spacetime.

Torsion Tensor

$$T^{\lambda}_{\mu\nu} = \Gamma^{\lambda}_{\nu\mu} - \Gamma^{\lambda}_{\mu\nu} \neq 0$$

Represents the antisymmetric part of the affine connection. The presence of torsion implies that infinitesimal parallelograms fail to close under parallel transport. In teleparallel gravity, torsion replaces curvature as the fundamental geometrical quantity describing the gravitational interaction.

J. M. Nester and H.-J. Yo, 1999

Curvature of Spacetime: Curvature vs Torsion

- The scalar curvature associated with the Levi–Civita connection can be written as

$$\mathcal{R}(\{\}) = -T + B,$$

where

$$T = \frac{1}{4} T_{\alpha\mu\nu} T^{\alpha\mu\nu} + \frac{1}{2} T_{\alpha\mu\nu} T^{\nu\mu\alpha} - T_\alpha T^\alpha,$$

and

$$B = 2\nabla_\mu T^\mu, \qquad T^\mu := T^{\nu\mu}{}_\nu.$$

- For a vanishing curvature of the Weitzenböck connection, a theory with Lagrangian density linear in $\mathcal{R}(\{\})$ is equivalent to a theory with Lagrangian density linear in T.
- The former statement does not apply to $f(\mathcal{R})$ and $f(T)$ because of the boundary term B.
- This gives rise to $f(T)$ gravity as a new avenue of exploration, particularly from a phenomenological perspective.

R. Aldrovandi and J. G. Pereira, (2013)

$f(T)$ gravity

- The gravitational action:

$$S = \int d^4x\, e \left[-\frac{1}{2} f(T) + \mathcal{L}_M \right].$$

- The equations of motion are deduced by varying the action with respect to the tetrad. In the covariant formulation, the inertial spin connection is also included to ensure local Lorentz invariance.
- The energy–momentum tensor for matter is conserved.

R. Ferraro and F. Fiorini, Phys. Rev. D **75**, 084031 (2007)

Y. F. Cai, S. Capozziello, M. De Laurentis and E. N. Saridakis, Rept. Prog. Phys. **79** (2016) no.10, 106901

S. Bahamonde, K. F. Dialektopoulos, C. Escamilla-Rivera, G. Farrugia, V. Gakis, M. Hendry, M. Hohmann, J. Levi Said, J. Mifsud and E. Di Valentino, Rept. Prog. Phys. **86** (2023) no.2, 026901

FLRW cosmology in $f(T)$ gravity

- The metric:

$$\mathrm{d}s^2 = -N^2(t)\,\mathrm{d}t^2 + a^2(t)\left[\mathrm{d}r^2 + r^2\left(\mathrm{d}\theta^2 + \sin^2\theta\,\mathrm{d}\phi^2\right)\right].$$

- The tetrad must be consistent with the symmetries of the FLRW spacetime. In the covariant formulation, an appropriate inertial spin connection must also be chosen to ensure local Lorentz invariance.
- There are infinitely many tetrads related by local Lorentz transformations that reproduce the same FLRW metric. Only those accompanied by the corresponding inertial spin connection are physically equivalent.
- From now on, we shall adopt the standard diagonal tetrad together with the corresponding inertial spin connection, which preserves the FLRW metric in its usual form.

R. Aldrovandi and J. G. Pereira, *Teleparallel Gravity* (Springer, 2013); M. Krššák and E. N. Saridakis, Class. Quantum Grav. 33 (2016) 115009.

Suitable $f(T)$ models for cosmology–1–

- Friedmann and Raychaudhuri equations:

$$6f_T H^2 - \frac{1}{2}f = \rho_m \qquad \left(12H^2 f_{TT} + f_T\right)\dot{H} = -\frac{1}{2}(\rho_m + p_m)\,.$$

- The conservation equation:

$$\dot{\rho}_m + 3H(\rho_m + p_m) = 0.$$

- Three potential candidates:

$$\begin{aligned} f_1(T) &= T\,\exp\left(\lambda\frac{T_0}{T}\right), \\ f_2(T) &= T + T_0\exp\left(-\lambda\frac{T_0}{T}\right), \\ f_3(T) &= T + \lambda T_0\left[1 - \exp\left(-\frac{T_0}{T}\right)\right]. \end{aligned}$$

- All these models can give rise to late-time cosmic acceleration.

R. Ferraro and F. Fiorini, Phys. Rev. D **75**, 084031 (2007); E. V. Linder, Phys. Rev. D **81**, 127301 (2010).

Suitable $f(\mathrm{T})$ models for cosmology-2-

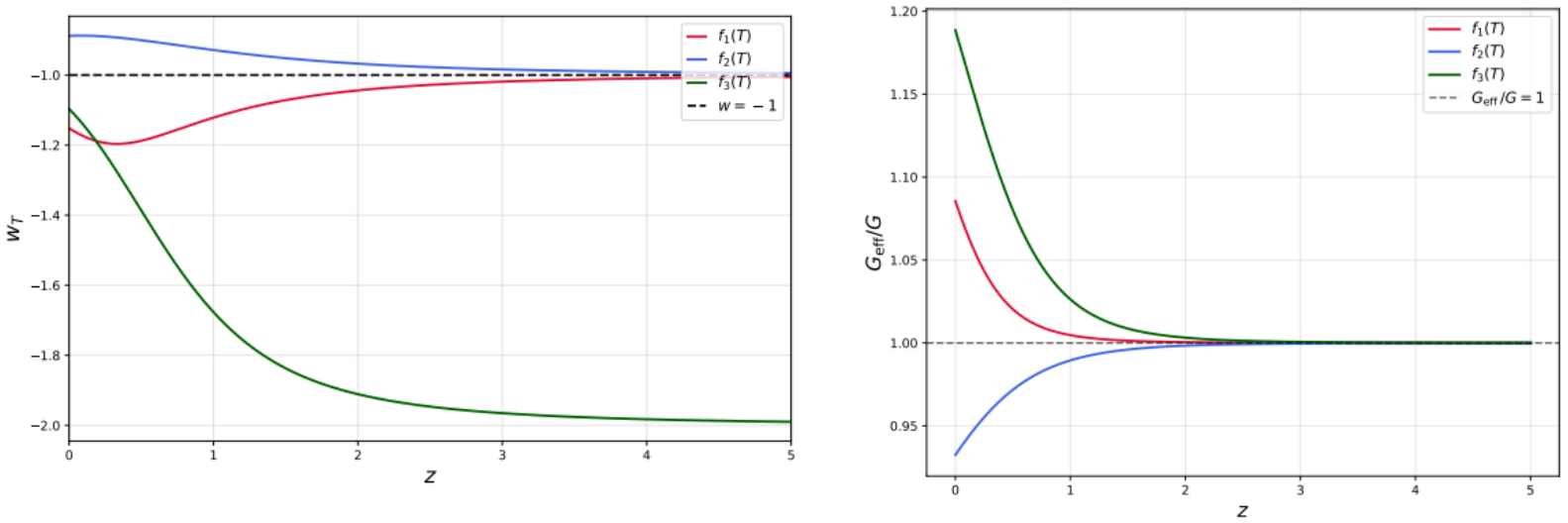

FIG. 1: *Cosmological background and effective sector of the $f(T)$ scenarios in comparison with ΛCDM.* ***Left panel:*** *Effective dark energy equation of state parameter $w_T(z)$ of the $f(T)$ models compared to ΛCDM ($w = -1$). Models 1 (crimson line) and 3 (green line) with $\lambda_1 = 0.36$ and $\lambda_3 = 0.42$ respectively, show phantom-like behaviour ($w_T < -1$), whereas Model 2 with $\lambda_2 = 0.09$ (blue line), lies in the quintessence regime ($w_T > -1$).* ***Right panel:*** *Effective Newton's constant $G_{\rm eff}/G$ as a function of the redshift z. Models 1 (crimson line) and 3 (green line) with $\lambda_1 = 0.36$, $\lambda_3 = 0.42$ respectively, show $G_{\rm eff} > G$, whereas Model 2 with $\lambda_2 = 0.09$ (blue line) exhibits $G_{\rm eff} < G$, with distinct implications for structure formation. The black dashed line $G_{\rm eff}/G = 1$ corresponds to the GR limit.*

M.B.-L, C.G. Boiza, M. Petronikolou and E. N. Saridakis, arXiv:2505.18264 (Universe)

Observational constraints

- The analysis is performed for five different combinations of datasets:
  - **Combination I:** Supernovae (SN);
  - **Combination II:** Baryon acoustic oscillations (BAO);
  - **Combination III:** Baryon acoustic oscillations and cosmic microwave background (BAO + CMB);
  - **Combination IV:** Redshift-space distortions (RSD)
  - **Combination V:** Full combination (SN + BAO+ CMB + RSD).

Fitting the model-1-

Model	H_0	Ω_{m0}	Ω_{b0}	S_8	χ^2_{min}	ΔAIC_C
			SN			
ΛCDM	73.28 ± 1.30	0.3321 ± 0.0186	0.04138 ± 0.00172	–	1402.9	–
$f_1(T)$	73.29 ± 1.26	0.3870 ± 0.0177	0.04136 ± 0.00175	–	1405.0	2.1
$f_2(T)$	73.24 ± 1.28	0.2792 ± 0.0136	0.04144 ± 0.00172	–	1402.5	−0.4
$f_3(T)$	73.24 ± 1.28	0.3862 ± 0.0197	0.04141 ± 0.00174	–	1403.5	0.6
			BAO			
ΛCDM	68.645 ± 0.505	0.29747 ± 0.00861	0.047173 ± 0.000728	–	10.3	–
$f_1(T)$	72.318 ± 0.542	0.29458 ± 0.00785	0.042475 ± 0.000673	–	20.1	9.8
$f_2(T)$	65.278 ± 0.529	0.30541 ± 0.00956	0.052180 ± 0.000812	–	9.1	−1.2
$f_3(T)$	72.654 ± 0.553	0.31003 ± 0.00819	0.042070 ± 0.000645	–	20.4	10.1
			BAO + CMB			
ΛCDM	68.401 ± 0.292	0.30111 ± 0.00374	0.048133 ± 0.000343	–	16.2	–
$f_1(T)$	71.963 ± 0.326	0.27621 ± 0.00350	0.043151 ± 0.000321	–	27.8	11.6
$f_2(T)$	64.850 ± 0.348	0.33107 ± 0.00483	0.053884 ± 0.000476	–	29.8	13.6
$f_3(T)$	72.317 ± 0.320	0.27778 ± 0.00345	0.042406 ± 0.000300	–	43.5	27.3
			RSD			
ΛCDM	–	0.2695 ± 0.0540	–	0.7423 ± 0.0378	11.94	–
$f_1(T)$	–	0.2604 ± 0.0521	–	0.7104 ± 0.0385	12.06	0.12
$f_2(T)$	–	0.2781 ± 0.0559	–	0.7695 ± 0.0430	11.96	0.02
$f_3(T)$	–	0.2444 ± 0.0499	–	0.6848 ± 0.0371	12.02	0.08
			SN + BAO + CMB + RSD			
ΛCDM	68.559 ± 0.278	0.29923 ± 0.00354	0.048014 ± 0.000326	0.7582 ± 0.0263	1447.8	–
$f_1(T)$	71.620 ± 0.322	0.28013 ± 0.00352	0.043475 ± 0.000315	0.7222 ± 0.0253	1486.8	39.0
$f_2(T)$	65.699 ± 0.316	0.31955 ± 0.00420	0.052873 ± 0.000426	0.7966 ± 0.0283	1492.4	44.6
$f_3(T)$	72.043 ± 0.305	0.28088 ± 0.00335	0.042649 ± 0.000293	0.7071 ± 0.0249	1494.1	46.3

TABLE III: Mean values and 1σ uncertainties of the cosmological parameters for the ΛCDM and $f(T)$ gravity models, obtained from individual datasets (SN, BAO, RSD) and from the combined BAO+CMB dataset, as well as from their full combination. For the RSD-only dataset, no constraints on H_0 and Ω_{b0} are reported, because these parameters are not directly constrained by RSD measurements alone. The column χ^2_{min} reports the minimum chi-square value at the best-fit point. The last column reports the Akaike Information Criterion difference, $\Delta AIC_C \equiv AIC_C^{f(T)} - AIC_C^{\Lambda CDM}$.

C.G. Boiza, M. Petronikolou, M.B.-L. and E. N. Saridakis: arXiv: 2601.22225 (Universe)

Fitting the model-2-

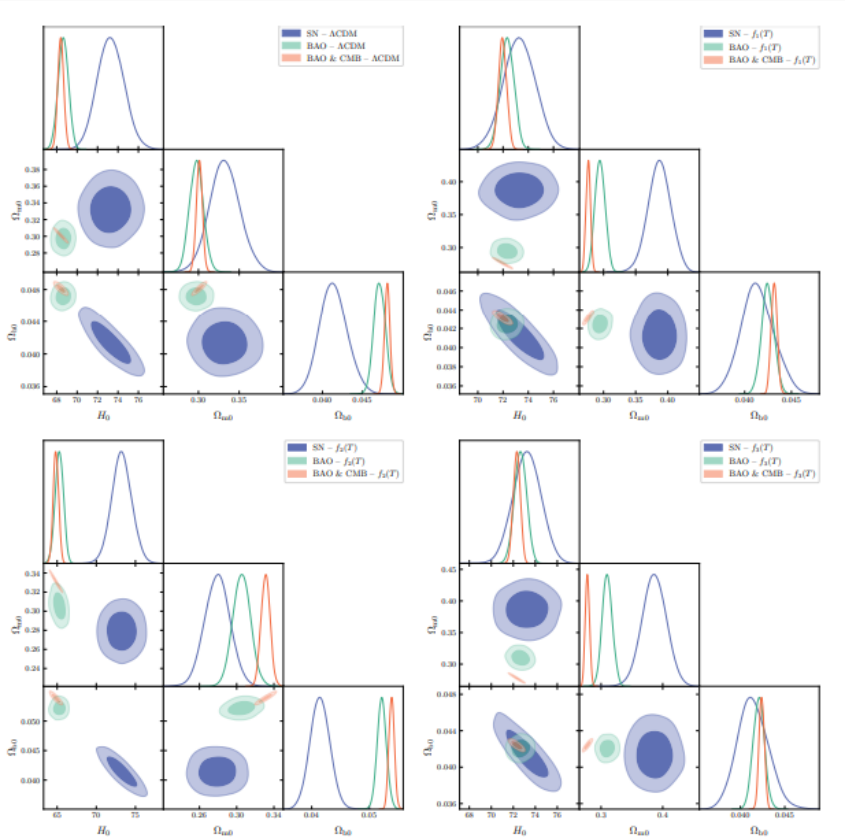

FIG. 2: *Comparison of the two-dimensional posterior distributions in the* (H_0, Ω_{m0}), (H_0, Ω_{b0}), *and* $(\Omega_{m0}, \Omega_{b0})$ *planes obtained from the individual SN, BAO, and BAO+CMB datasets. The contours correspond to the 68% and 95% confidence levels (C.L.). The top-left panel shows the results for the ΛCDM model, while the remaining panels correspond to the* $f_1(T)$ *(top-right),* $f_2(T)$ *(bottom-left), and* $f_3(T)$ *(bottom-right) models. The relative displacement and overlap of the contours reveal the presence of internal tensions among the datasets for each model.*

C.G. Boiza, M. Petronikolou, M.B.-L. and E. N. Saridakis: arXiv: 2601.22225 (Universe)

Fitting the model-3-

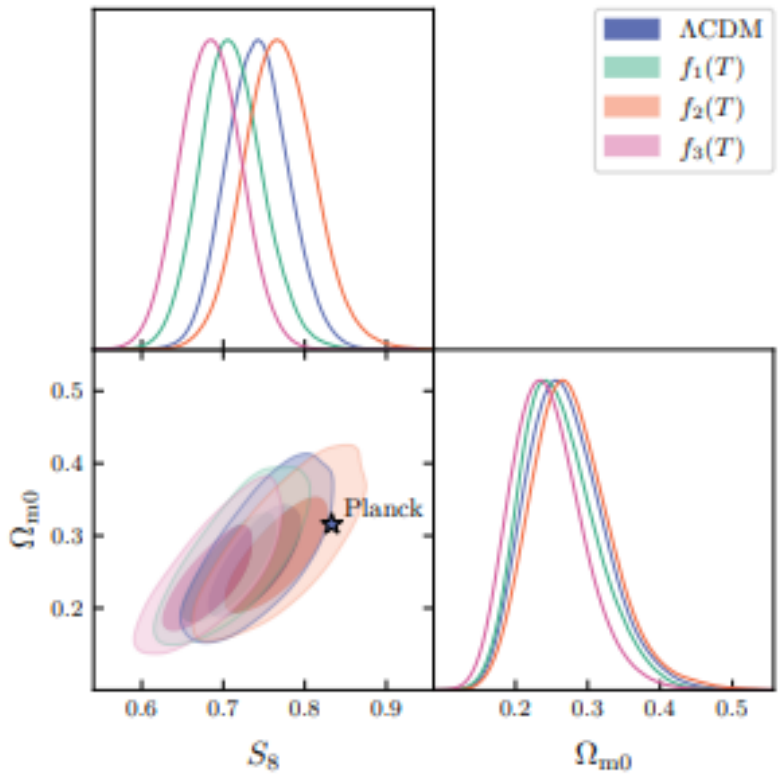

FIG. 3: *Two-dimensional posterior distributions in the* (Ω_{m0}, S_8) *plane obtained from the RSD dataset. The contours correspond to the 68% and 95% confidence levels (C.L.) for the* ΛCDM *and* $f(T)$ *gravity models. For reference, the Planck 2018 best-fit constraint [7] is also shown.*

C.G. Boiza, M. Petronikolou, M.B.-L. and E. N. Saridakis: arXiv: 2601.22225 (Universe)

Fitting the model-4-

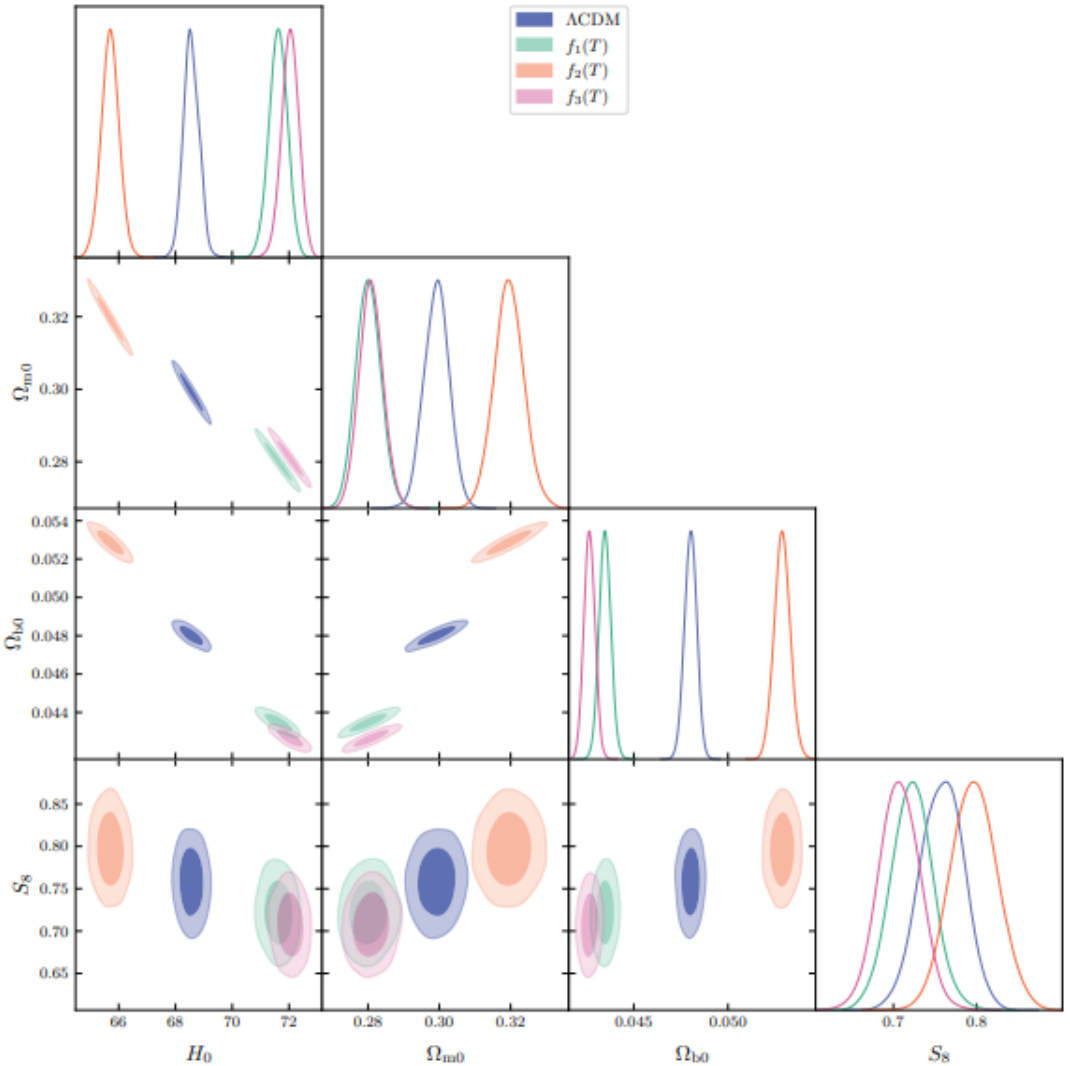

FIG. 4: *Two-dimensional posterior distributions for the ΛCDM and $f(T)$ gravity models obtained from the full dataset combination (SN + BAO + CMB + RSD). The contours correspond to the 68% and 95% confidence levels (C.L.). The figure displays all one- and two-dimensional marginalised constraints among the parameters H_0, Ω_{m0}, Ω_{b0}, and S_8. Differences in the location of the contours illustrate how the various $f(T)$ parametrisations modify the joint parameter constraints relative to the ΛCDM scenario.*

Can the presence of Λ improve these fits?-1-

Parameter	SNe + low-z	BAO	BAO + CMB	RSD	Full combination
			ΛCDM		
H_0	73.3 ± 1.3	68.65 ± 0.51	68.40 ± 0.29	> 68.1	68.56 ± 0.28
Ω_{m0}	0.332 ± 0.019	0.2975 ± 0.0086	0.3011 ± 0.0037	$0.270^{+0.044}_{-0.061}$	0.2992 ± 0.0035
Ω_{b0}	$0.0414^{+0.0016}_{-0.0018}$	0.04717 ± 0.00073	0.04813 ± 0.00034	$0.05007^{+0.00084}_{-0.030}$	0.04801 ± 0.00033
Ω_Λ	0.668 ± 0.019	0.7024 ± 0.0086	0.6988 ± 0.0037	$0.730^{+0.061}_{-0.044}$	0.7007 ± 0.0035
σ_8	–	–	–	$0.792^{+0.053}_{-0.062}$	0.759 ± 0.027
S_8	–	–	–	0.742 ± 0.038	0.758 ± 0.026
AICc	1408.93	18.95	24.21	22.29	1455.82
BIC	1425.24	17.98	24.53	24.30	1477.64
DIC	1407.06 ± 0.13	14.260 ± 0.060	22.132 ± 0.059	16.05 ± 0.11	1455.58 ± 0.24
WAIC	1407.12 ± 0.27	14.356 ± 0.072	22.173 ± 0.068	16.00 ± 0.18	1455.44 ± 0.23
$-\ln B$	1407.83 ± 0.52	15.66 ± 0.99	22.22 ± 0.54	16.34 ± 0.40	1455.20 ± 0.62
			$f_1(Q) + \Lambda$		
H_0	73.2 ± 1.3	$66.1^{+2.2}_{-2.0}$	$68.9^{+1.1}_{-0.97}$	> 70.8	68.74 ± 0.55
Ω_{m0}	$0.288^{+0.050}_{-0.079}$	$0.3044^{+0.0088}_{-0.012}$	$0.2975^{+0.0073}_{-0.0088}$	$0.257^{+0.056}_{-0.066}$	0.2980 ± 0.0048
Ω_{b0}	0.0415 ± 0.0018	$0.0510^{+0.0027}_{-0.0037}$	$0.0474^{+0.0013}_{-0.0016}$	$0.04647^{+0.00021}_{-0.028}$	0.04774 ± 0.00080
$\Omega_{cJ}(z=0)$	$0.66^{+0.33}_{-1.0}$	$0.77^{+0.21}_{-0.17}$	1.049 ± 0.091	$1.05^{+0.33}_{-1.4}$	1.019 ± 0.050
Ω_Λ	$0.05^{+1.1}_{-0.57}$	$-0.07^{+0.16}_{-0.20}$	-0.347 ± 0.083	$-0.30^{+1.3}_{-0.57}$	-0.317 ± 0.047
$\tilde{\Omega}_\Lambda$	$1.05^{+1.1}_{-0.57}$	$0.93^{+0.16}_{-0.20}$	0.653 ± 0.083	$0.70^{+1.3}_{-0.57}$	0.683 ± 0.047
λ_1	$0.2020^{+0.0083}_{-0.30}$	$0.088^{+0.055}_{-0.085}$	$-0.016^{+0.027}_{-0.032}$	$0.09^{+0.16}_{-0.50}$	-0.006 ± 0.017
σ_8	–	–	–	$0.793^{+0.068}_{-0.080}$	0.759 ± 0.028
S_8	–	–	–	$0.726^{+0.13}_{-0.089}$	0.757 ± 0.028
$\mathrm{AIC_C}$	1410.30	21.79	27.53	25.68	1457.73
BIC	1432.04	19.05	26.99	27.39	1485.00
DIC	1408.81 ± 0.16	14.84 ± 0.15	23.83 ± 0.12	16.374 ± 0.064	1457.76 ± 0.41
WAIC	1408.64 ± 0.40	14.91 ± 0.40	23.83 ± 0.22	16.06 ± 0.10	1457.52 ± 0.63
$-\ln B$	1409.94 ± 0.58	15.19 ± 0.25	24.09 ± 0.49	16.94 ± 0.55	1458.4 ± 2.7
			Differences relative to ΛCDM		
$\Delta\mathrm{AIC_C}$	1.37	2.84	3.32	3.39	1.91
ΔBIC	6.80	1.07	2.46	3.09	7.36
ΔDIC	1.75 ± 0.21	0.58 ± 0.16	1.70 ± 0.13	0.32 ± 0.13	2.18 ± 0.48
ΔWAIC	1.52 ± 0.48	0.55 ± 0.41	1.66 ± 0.23	0.06 ± 0.21	2.08 ± 0.67
$\Delta(-\ln B)$	2.11 ± 0.78	-0.5 ± 1.0	1.87 ± 0.73	0.60 ± 0.68	3.2 ± 2.8

TABLE IV: Summary of the observational constraints obtained for ΛCDM and the modified gravity model $f_1(Q) + \Lambda$, using the different dataset combinations considered in this work: SNe+low-z, BAO, BAO+CMB, RSD, and the full combined dataset. Reported parameter constraints correspond to posterior mean values and 68% credible intervals. Parameters that are unconstrained or only weakly constrained are omitted. The table also reports the model comparison statistics $\mathrm{AIC_C}$, BIC, DIC, WAIC, and $-\ln B$, together with their differences relative to ΛCDM. Positive values of $\Delta\mathrm{AIC_C}$, ΔBIC, ΔDIC, ΔWAIC, and $\Delta(-\ln B)$ indicate that the corresponding modified gravity model is disfavoured relative to ΛCDM, according to the convention adopted in Section V C.

M.B.-L, C.G. Boiza, M. Petronikolou and E. N. Saridakis: arXiv:2607.XXXXX

Can the presence of Λ improve these fits?-2-

Parameter	SNe + low-z	BAO	BAO + CMB	RSD	Full combination
			ΛCDM		
H_0	73.3 ± 1.3	68.65 ± 0.51	68.40 ± 0.29	> 68.1	68.56 ± 0.28
Ω_{m0}	0.332 ± 0.019	0.2975 ± 0.0086	0.3011 ± 0.0037	$0.270^{+0.044}_{-0.061}$	0.2992 ± 0.0035
Ω_{b0}	$0.0414^{+0.0016}_{-0.0018}$	0.04717 ± 0.00073	0.04813 ± 0.00034	$0.05007^{+0.00084}_{-0.030}$	0.04801 ± 0.00033
Ω_Λ	0.668 ± 0.019	0.7024 ± 0.0086	0.6988 ± 0.0037	$0.730^{+0.061}_{-0.044}$	0.7007 ± 0.0035
σ_8	–	–	–	$0.792^{+0.053}_{-0.062}$	0.759 ± 0.027
S_8	–	–	–	0.742 ± 0.038	0.758 ± 0.026
AICc	1408.93	18.95	24.21	22.29	1455.82
BIC	1425.24	17.98	24.53	24.30	1477.64
DIC	1407.06 ± 0.13	14.260 ± 0.060	22.132 ± 0.059	16.05 ± 0.11	1455.58 ± 0.24
WAIC	1407.12 ± 0.27	14.356 ± 0.072	22.173 ± 0.068	16.00 ± 0.18	1455.44 ± 0.23
$-\ln B$	1407.83 ± 0.52	15.66 ± 0.99	22.22 ± 0.54	16.34 ± 0.40	1455.20 ± 0.62
			$f_2(Q) + \Lambda$		
H_0	73.2 ± 1.3	67.4 ± 1.6	69.19 ± 0.71	> 68.9	69.08 ± 0.54
Ω_{m0}	$0.373^{+0.060}_{-0.12}$	$0.2948^{+0.0088}_{-0.0088}$	0.2960 ± 0.0056	0.235 ± 0.070	0.2962 ± 0.0044
Ω_{b0}	0.0414 ± 0.0017	0.0489 ± 0.0024	0.0469 ± 0.0010	$0.0488^{-0.0011}_{-0.027}$	0.04717 ± 0.00079
$\Omega_Q(z=0)$	$0.47^{+0.50}_{-1.4}$	-0.19 ± 0.25	0.14 ± 0.11	$0.66^{+0.67}_{-1.6}$	0.103 ± 0.088
Ω_Λ	$0.15^{+1.5}_{-0.64}$	0.90 ± 0.25	0.57 ± 0.11	$0.10^{+1.5}_{-0.71}$	0.600 ± 0.086
λ_2	$0.35^{+0.43}_{-0.88}$	-0.14 ± 0.18	0.100 ± 0.082	$0.48^{+0.49}_{-1.1}$	0.076 ± 0.064
σ_8	–	–	–	$0.779^{+0.055}_{-0.071}$	0.757 ± 0.027
S_8	–	–	–	$0.679^{+0.13}_{-0.089}$	0.752 ± 0.027
$\mathrm{AIC_C}$	1410.32	22.51	26.55	25.68	1456.59
BIC	1432.05	19.77	26.00	27.38	1483.86
DIC	1408.529 ± 0.082	15.50 ± 0.15	22.89 ± 0.18	16.1005 ± 0.0026	1456.378 ± 0.042
WAIC	1407.7309 ± 0.0046	15.59 ± 0.33	22.9969 ± 0.0086	16.11 ± 0.12	1456.19 ± 0.16
$-\ln B$	1407.626 ± 0.083	16.8 ± 1.3	24.1 ± 1.2	16.56 ± 0.58	1456.12 ± 0.10
			Differences relative to ΛCDM		
$\Delta\mathrm{AIC_C}$	1.39	3.56	2.34	3.39	0.77
ΔBIC	6.81	1.79	1.47	3.08	6.22
ΔDIC	1.47 ± 0.15	1.24 ± 0.16	0.76 ± 0.19	0.05 ± 0.11	0.80 ± 0.24
ΔWAIC	0.61 ± 0.27	1.23 ± 0.34	0.824 ± 0.069	0.11 ± 0.22	0.75 ± 0.28
$\Delta(-\ln B)$	-0.20 ± 0.53	1.1 ± 1.6	1.9 ± 1.3	0.22 ± 0.70	0.92 ± 0.63

TABLE V: Summary of the observational constraints obtained for ΛCDM and the modified gravity model $f_2(Q) + \Lambda$, using the different dataset combinations considered in this work: SNe+low-z, BAO, BAO+CMB, RSD, and the full combined dataset. Reported parameter constraints correspond to posterior mean values and 68% credible intervals. Parameters that are unconstrained or only weakly constrained are omitted. The table also reports the model comparison statistics $\mathrm{AIC_C}$, BIC, DIC, WAIC, and $-\ln B$, together with their differences relative to ΛCDM. Positive values of $\Delta\mathrm{AIC_C}$, ΔBIC, ΔDIC, ΔWAIC, and $\Delta(-\ln B)$ indicate that the corresponding modified gravity model is disfavoured relative to ΛCDM, according to the convention adopted in Section V C.

M.B.-L, C.G. Boiza, M. Petronikolou and E. N. Saridakis: arXiv:arXiv:2607.XXXXX

Fitting the model-1-

Model	GoF	ΔGoF	S	ΔS	$-\ln \mathrm{R}$	$\Delta(-\ln \mathrm{R})$
ΛCDM	$3.89 \pm 0.15\sigma$	–	$3.63 \pm 0.19\sigma$	–	12.29 ± 0.80	–
$f_1(Q) + \Lambda$	$3.692 \pm 0.091\sigma$	$-0.20 \pm 0.18\sigma$	$3.28 \pm 0.11\sigma$	$-0.35 \pm 0.22\sigma$	9.7 ± 2.9	-2.6 ± 3.0
$f_2(Q) + \Lambda$	$3.844 \pm 0.070\sigma$	$-0.05 \pm 0.17\sigma$	$3.443 \pm 0.088\sigma$	$-0.19 \pm 0.21\sigma$	11.00 ± 0.36	-1.29 ± 0.88

TABLE VI: Comparison of the goodness of fit (GoF), suspiciousness statistic S, and Bayes ratio between the BAO+CMB and SNe+low-z datasets for ΛCDM and the two modified gravity models $f_1(Q) + \Lambda$ and $f_2(Q) + \Lambda$. The quantities ΔGoF, ΔS, and $\Delta(-\ln \mathrm{R})$ denote the differences relative to ΛCDM. Positive values indicate a larger level of discordance between the two datasets than in ΛCDM, while negative values indicate improved concordance.

C.G. Boiza, M. Petronikolou, M.B.-L. and E. N. Saridakis: arXiv: 2601.22225 (Universe)

Speeding up with fields

Speeding up with fields

Quintessence through a genealised axion-like potential

Quintessence

- Minimally coupled canonical scalar field:

$$L = \frac{1}{2k^2}R - \frac{1}{2}g^{\mu\nu}\nabla_\mu\phi\nabla_\nu\phi - V(\phi) + L_{r,m}.$$

  - ϕ is a dynamical field.
  - **Coincidence problem.** It can be alleviated by scaling solutions and tracker fields.
  - Fine-tuning problem remains unsolved.
  - Some quintessence models allow for a natural explanation of why now?
  - Could the tensions H_0 and S_8 been alleviated?
- An axion-like potential: $V(\phi) = \Lambda^4[1 - \cos(\phi/\eta)]^{-n}$ with a generalisation to negative exponents, i.e. $0 < n$.
- Previously analised on the context of wave dark matter and early dark energy *Wave Dark Matter* (L. Hui). [arXiv:2101.11735], *Dark energy from the string axiverse* (M. Kamionkowski). [arXiv:1409.0549]

This part of the pat of the talk is based on C.G. Boiza, M.B.-L, H.-W. Chiang, 2409.18184 (EPJC), 2410.22467 (Phys. Dark Univ), 2503.04898 (JCAP)

Dynamical system

- Dynamical variables (FLRW filled by rad., mat. and an axion-like field):

$$x = \frac{k\dot{\phi}}{\sqrt{6}H}, \quad y = \frac{k\sqrt{V}}{\sqrt{3}H}, \quad \lambda = -\frac{V_{,\phi}}{kV}, \quad z = \Omega_r^{1/2} = \frac{k\sqrt{\rho_r}}{\sqrt{3}H}.$$

- Matter part: $\Omega_m = 1 - x^2 - y^2 - z^2$.
- Autonomous closed system of equations:

$$x' = \frac{1}{2}\left[-3x + 3x^3 - 3xy^2 + xz^2\right] + \sqrt{\frac{3}{2}}\lambda y^2,$$

$$y' = \frac{1}{2}\left[3y - 3y^3 + 3yx^2 + yz^2\right] - \sqrt{\frac{3}{2}}\lambda xy,$$

$$z' = \frac{1}{2}\left[-z + z^3 + 3zx^2 - 3zy^2\right],$$

$$\lambda' = -\sqrt{6}f(\lambda)x, \qquad f(\lambda) = \lambda^2[\Gamma(\lambda) - 1], \qquad \Gamma = \frac{V_{,\phi\phi}V}{(V_{,\phi})^2}$$

Fixed points

Point	x	y	z	λ	w_{eff}	Stability
A_1	0	0	0	Any	0	Saddle
A_2	0	0	1	Any	$1/3$	Saddle
E	0	1	0	0	-1	(Un)Stable if $n > 0$ ($n < 0$)

Tracking behaviour

Unique evolution of ϕ. It does not depend on the initial conditions.

Tracking regime given by $\omega_\phi \approx const.$

- Tracking with $\omega_\phi > \omega$: it could happen, but it is disregarded (structure formation suppression). Here ω stands for EoS of radiation or matter.
- **Tracking with $\omega_\phi < \omega$: $\Gamma > 1$ and $\Gamma \approx const.$ in the regime $\lambda \gg 1$.**

$$\omega_\phi = \frac{\omega - 2(\Gamma - 1)}{1 + 2(\Gamma - 1)}.$$

Axion-like potential

$$V(\phi) = \Lambda^4[1 - \cos(\phi/\eta)]^{-n}.$$

Generalisation to $n > 0$

$$\lambda(\phi) = \frac{n}{k\eta}\frac{\sin(\phi/\eta)}{1-\cos(\phi/\eta)}$$

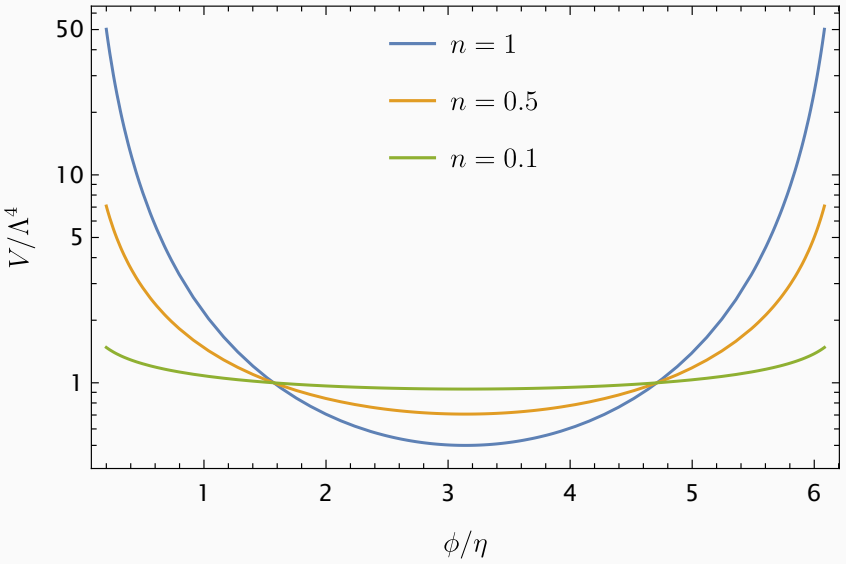

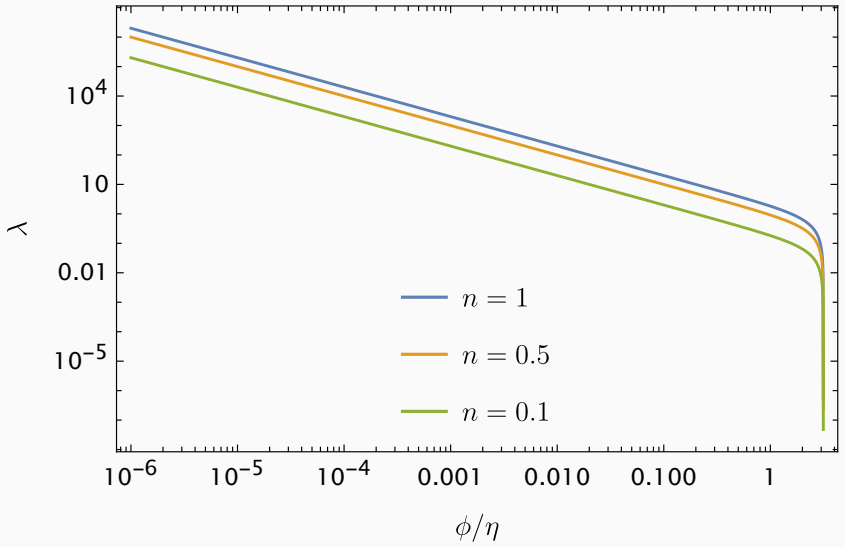

- Cosmological constant in the limit $n \to 0$.
- Minimum at $\phi/\eta = \pi \to V \approx V_{\min} + \frac{1}{2}m^2(\phi - \pi\eta)^2$ where $V_{\min} \equiv \Lambda^4/2^n$ and $m^2 \equiv n\Lambda^4/(2^{n+1}\eta^2)$.
- $\phi_{ini}/\eta \ll 1$ in order to have non-trivial evolution $\to \lambda_{ini} \gg 1$.

Fixed points and tracking

- Fixed points: A_1, A_2 and E (minimum of the potential). E is an attractor $\rightarrow$ **Late-time acceleration.**
- $\Gamma(\lambda) = 1 + \frac{1}{2n} + \frac{n}{2k^2\eta^2\lambda^2}$. In the regime $\lambda \gg 1$: $\Gamma \approx 1 + \frac{1}{2n} \rightarrow$ **Tracking behaviour** with $\omega_\phi < \omega$.
- Tracking regime given by $\omega_\phi \approx -\frac{2(\Gamma-1)}{1+2(\Gamma-1)} = -\frac{1}{1+n} \quad (\omega = 0)$.

$n = 1, \quad \omega_\phi \approx -0.5$

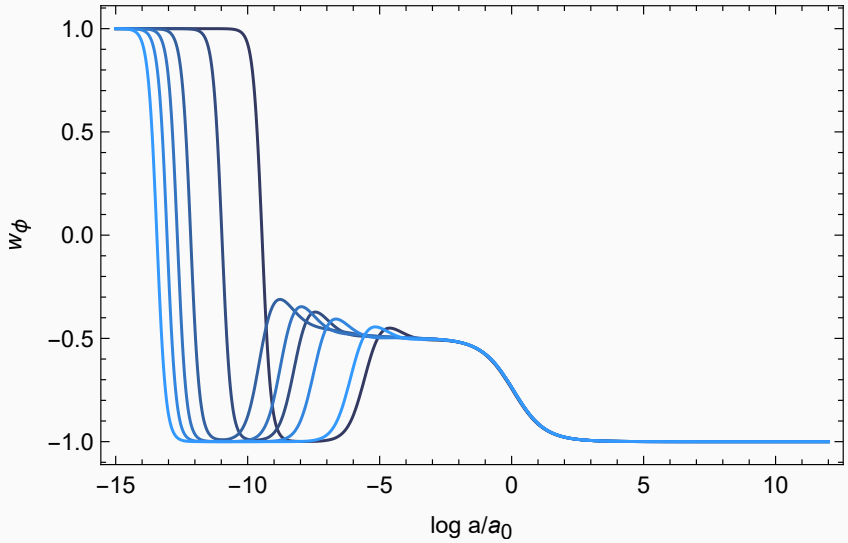

$n = 0.1, \quad \omega_\phi \approx -0.9$

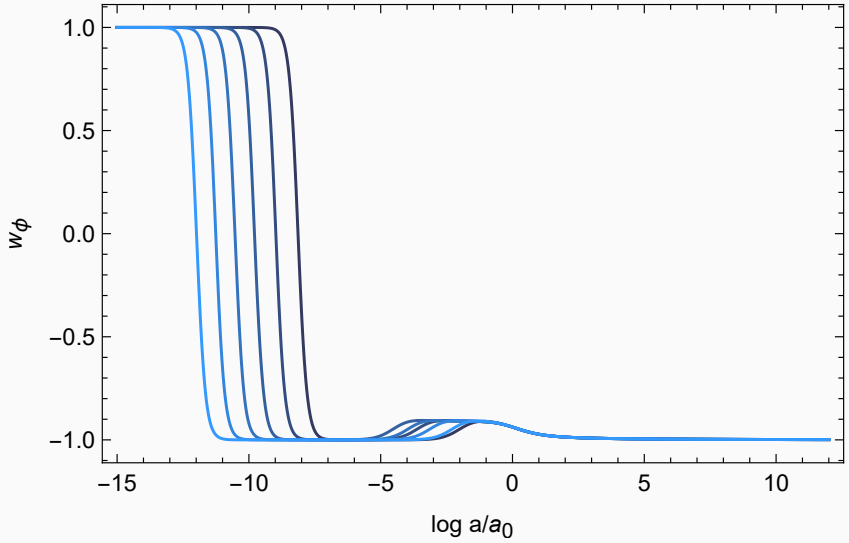

Matter power spectrum

Matter power spectrum suppression:

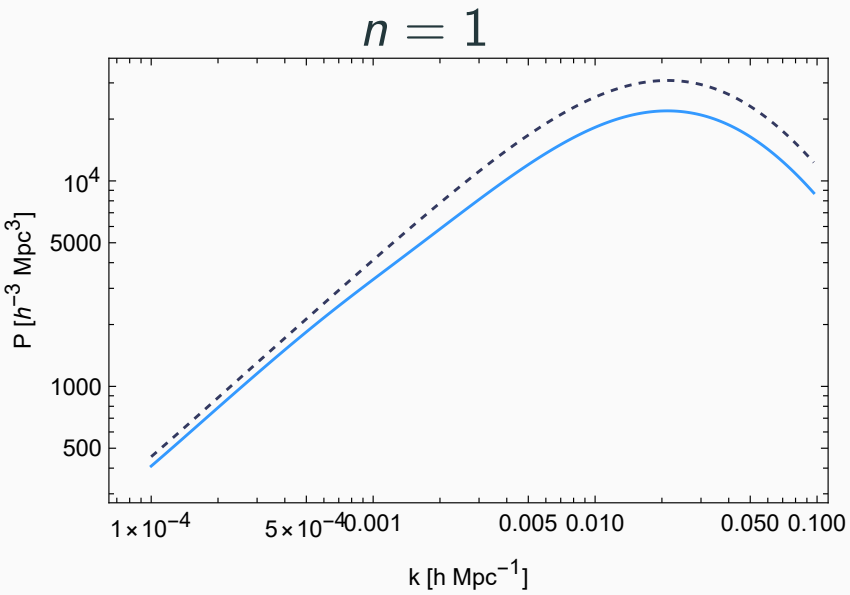

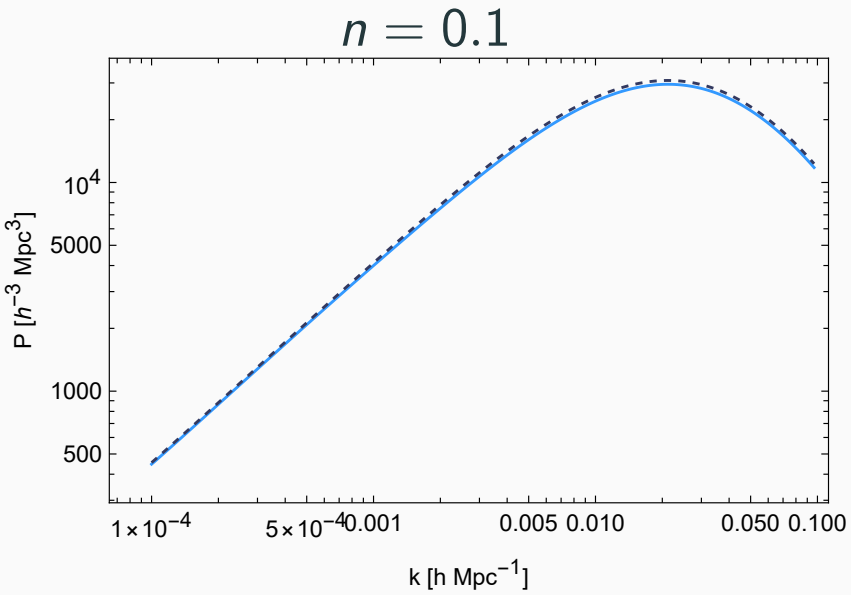

fσ8 behaviour

fσ8 distribution:

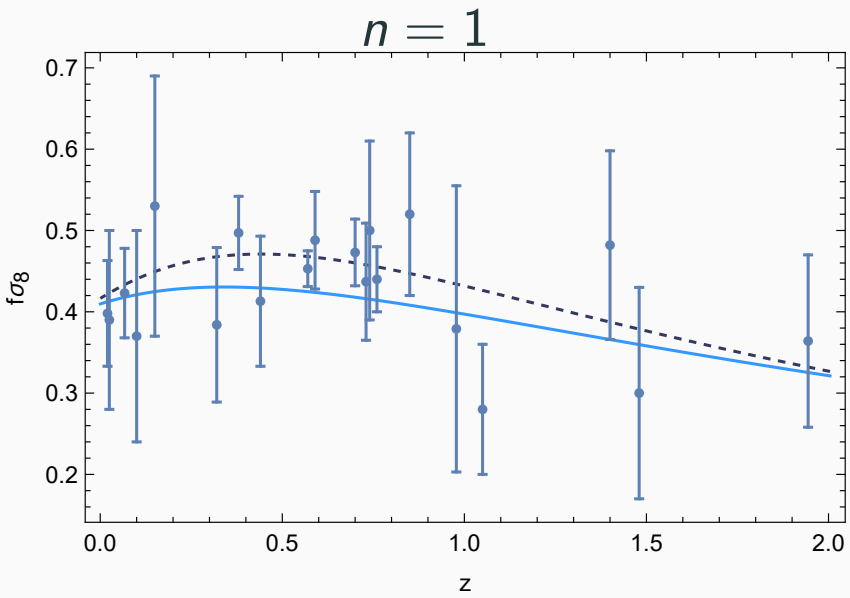

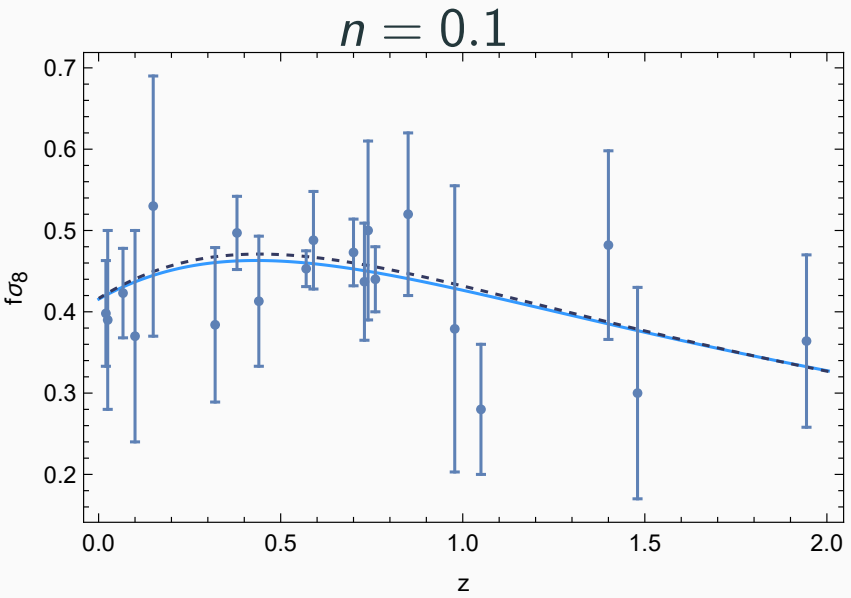

Fitting the model-1-

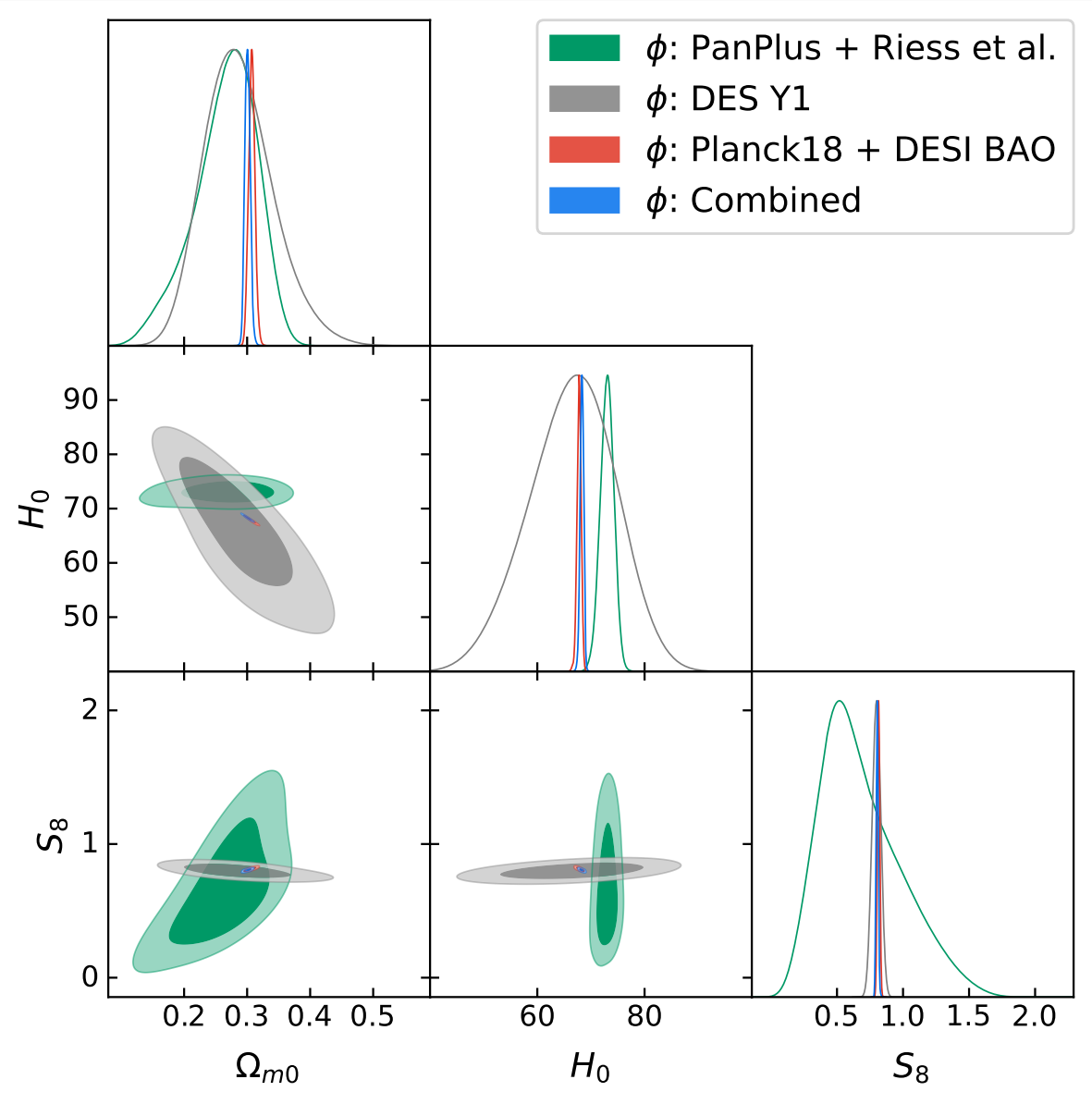

H.-W. Chiang, C.G. Boiza and M.B.-L.: arxiv:2503.04898 (JCAP)

Comparing the model

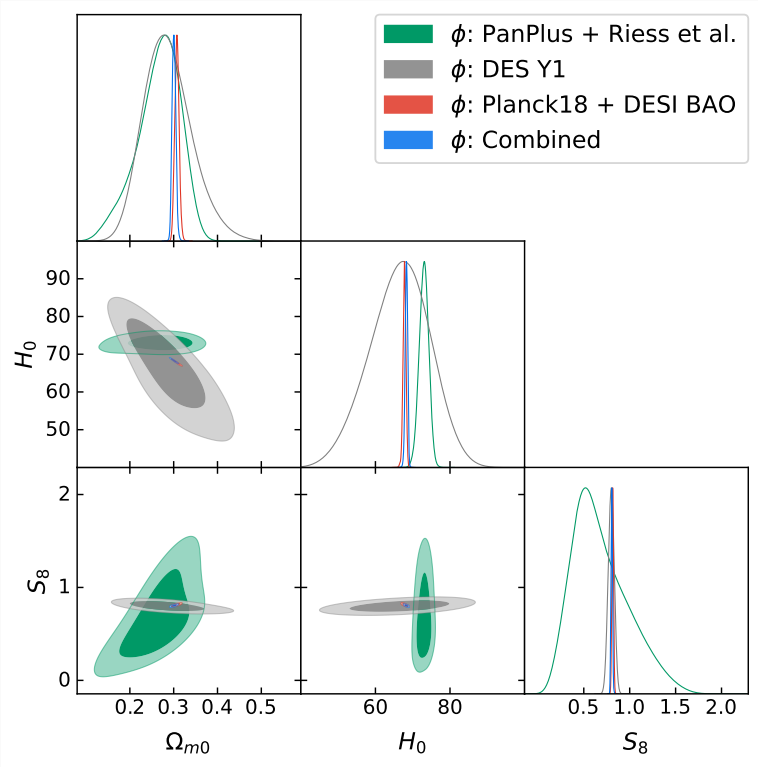

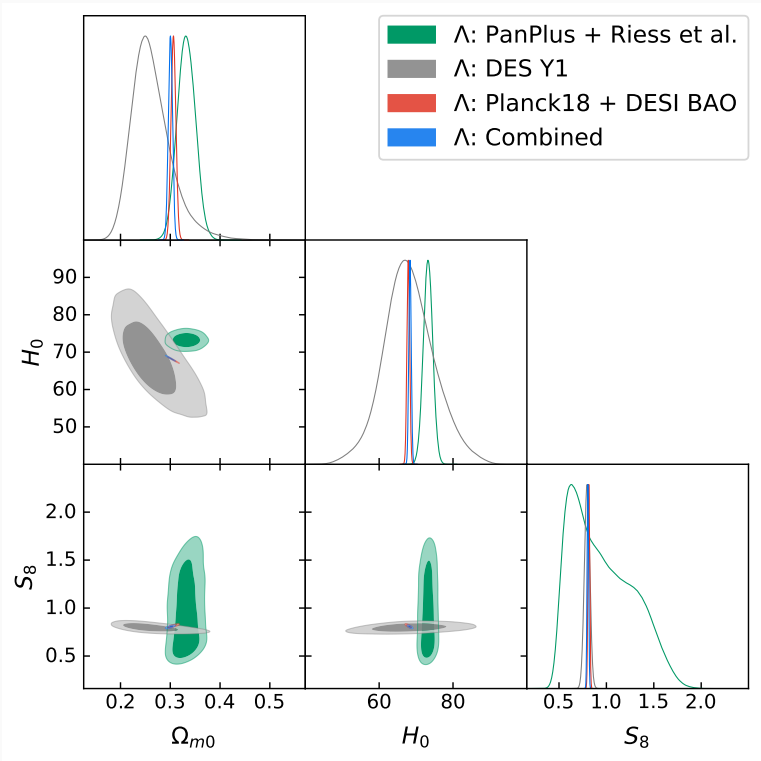

Fitting the model-2-

	CMB	+ BAO	+ SNe	+ low-z	+ DES Y1
$10^3\Omega_{b0}h^2$	22.19 ± 0.13	22.29 ± 0.12	22.26 ± 0.12	22.34 ± 0.12	22.38 ± 0.12
$10^3\Omega_{c0}h^2$	119.7 ± 1.0	118.26 ± 0.81	118.56 ± 0.79	117.80 ± 0.76	117.27 ± 0.72
$10^5\theta_{\rm MC}$	1040.77 ± 0.25	1040.94 ± 0.24	1040.91 ± 0.24	1041.01 ± 0.24	1041.05 ± 0.24
$\ln(10^{10}A_s)$	3.037 ± 0.014	3.044 ± 0.014	3.043 ± 0.014	3.047 ± 0.014	3.046 ± 0.014
n_s	0.9636 ± 0.0040	0.9672 ± 0.0036	0.9665 ± 0.0036	0.9685 ± 0.0036	0.9693 ± 0.0036
$\tau_{\rm reio}$	0.0524 ± 0.0071	0.0571 ± 0.0071	0.0562 ± 0.0070	0.0587 ± 0.0071	0.0589 ± 0.0071
H_0	67.24 ± 0.46	67.89 ± 0.36	67.76 ± 0.35	68.12 ± 0.34	68.36 ± 0.32
Ω_{m0}	0.3154 ± 0.0064	0.3064 ± 0.0048	0.3082 ± 0.0047	0.3034 ± 0.0044	0.3003 ± 0.0042
σ_8	0.8077 ± 0.0055	0.8064 ± 0.0056	0.8067 ± 0.0056	0.8061 ± 0.0057	0.8041 ± 0.0055
S_8	0.828 ± 0.011	0.8149 ± 0.0090	0.8176 ± 0.0090	0.8107 ± 0.0087	0.8044 ± 0.0080
DIC	5497.90 ± 0.12	5507.21 ± 0.37	6209.34 ± 0.14	6217.77 ± 0.43	6477.38 ± 0.28
WAIC	5499.09 ± 0.50	5507.85 ± 0.18	6210.36 ± 0.21	6218.68 ± 0.21	6481.16 ± 0.22
$-\ln B$	5499.3 ± 1.1	5508.13 ± 0.73	6210.51 ± 0.44	6219.1 ± 1.4	6479.9 ± 1.2

Table 2. Mean and standard deviation of cosmological parameters, late-time observables, and statistical probes for ΛCDM model. From left to right are gradually larger datasets that progressively add in datasets of CMB, BAO, etc., as defined in section 3.1.

	CMB	+ BAO	+ SNe	+ low-z	+ DES Y1
$10^3\Omega_{b0}h^2$	22.18 ± 0.13	22.28 ± 0.12	22.28 ± 0.12	22.34 ± 0.12	22.39 ± 0.12
$10^3\Omega_{c0}h^2$	119.8 ± 1.1	118.29 ± 0.80	118.40 ± 0.83	117.73 ± 0.79	117.22 ± 0.73
$10^5\theta_{\rm MC}$	1040.76 ± 0.25	1040.95 ± 0.24	1040.93 ± 0.24	1041.03 ± 0.23	1041.06 ± 0.26
$\ln(10^{10}A_s)$	3.039 ± 0.014	3.044 ± 0.014	3.044 ± 0.014	3.048 ± 0.014	3.048 ± 0.014
n_s	0.9634 ± 0.0040	0.9671 ± 0.0036	0.9669 ± 0.0037	0.9686 ± 0.0036	0.9694 ± 0.0035
$\tau_{\rm reio}$	0.0532 ± 0.0071	0.0568 ± 0.0073	0.0566 ± 0.0071	0.0590 ± 0.0072	0.0596 ± 0.0073
$\log_{10}(\rho_{\rm DE,0}/V_{\rm min} - 1)$	$-2.9^{+2.1}_{-0.7}$	$-2.92^{+0.45}_{-0.75}$	$-3.0^{+2.6}_{-0.6}$	$-2.94^{+0.43}_{-0.76}$	$-3.0^{+3.1}_{-0.8}$
$\log_{10}(\eta/M_P)$	$-1.25^{+0.31}$	$-2.0^{+0.8}$	-0.8	$-2.0^{+0.7}$	-0.8
n	$0^{+0.6}$	$0^{+0.6}$	$0^{+0.5}$	$0^{+0.6}$	$0^{+0.6}$
$\log_{10}(\phi_i/\eta)$	$0.5_{-3.3}$	$0.5_{-3.0}$	$0.5_{-2.0}$	$0.5_{-2.9}$	$0.5_{-1.5}$
H_0	$67.05^{+0.62}_{-0.77}$	67.77 ± 0.39	67.62 ± 0.45	68.08 ± 0.36	68.31 ± 0.33
Ω_{m0}	$0.3177^{+0.0095}_{-0.0078}$	0.3075 ± 0.0049	0.3091 ± 0.0053	0.3036 ± 0.0046	0.3006 ± 0.0042
σ_8	$0.8056^{+0.0070}_{-0.0079}$	0.8049 ± 0.0062	0.8042 ± 0.0067	0.8052 ± 0.0059	0.8035 ± 0.0059
S_8	0.831 ± 0.012	0.8149 ± 0.0091	0.8163 ± 0.0090	0.8100 ± 0.0089	0.8042 ± 0.0080
DIC	5498.13 ± 0.54	5507.87 ± 0.13	6210.08 ± 0.35	6218.58 ± 0.01	6478.21 ± 0.53
WAIC	5499.03 ± 0.53	5508.42 ± 0.15	6210.85 ± 0.03	6219.12 ± 0.29	6481.97 ± 0.92
$-\ln B$	5499.74 ± 0.99	5509.2 ± 2.4	6210.17 ± 0.04	6219.09 ± 0.20	6482.8 ± 2.8
ΔDIC	0.23 ± 0.59	0.66 ± 0.41	0.74 ± 0.39	0.81 ± 0.51	0.83 ± 0.63
ΔWAIC	-0.06 ± 0.77	0.56 ± 0.24	0.48 ± 0.45	0.43 ± 0.39	0.81 ± 0.97
$-\Delta \ln B$	0.4 ± 1.6	1.0 ± 2.4	-0.35 ± 0.52	-0.1 ± 1.7	2.9 ± 3.2

Table 3. Mean and standard deviation of cosmological parameters, late-time observables, and statistical probes for the axion-like dark energy model in section 2. From left to right are gradually larger datasets of CMB, CMB + BAO, CMB + BAO + SNe, etc., as defined in section 3.1. ΔICs are with respect to ΛCDM model presented in table 2. For parameters not following Gaussian distribution we provide the median and 68% lower and upper bounds (if valid) instead, with color coding for how heavy the tail is (red for short tail, black for Gaussian, blue for exponential, and cyan for long tail.) For single-sided distributions we report the modal and the single-sided 68% bound instead.

H.-W. Chiang, C.G. Boiza and M.B.-L.: arxiv:2503.04898 (JCAP)

Fitting the model-3-

	BAO	SNe + low-z	DES Y1
$10^3\Omega_{c0}h^2$	111 ± 11	116 ± 29	107^{+15}_{-19}
$10^5\theta_{MC}$	1036 ± 12	1081^{+15}_{-18}	1048^{+36}_{-38}
$\ln(10^{10}A_s)$			$3.47^{+0.27}_{-0.29}$
$\log(\rho_{DE,0}/V_{min} - 1)$	$-2.8^{+2.1}_{-0.6}$	$-0.08^{+0.80}_{-0.95}$	$-1.0^{+1.8}_{-1.6}$
$\log(\eta/M_P)$	$-0.89^{+0.56}$	$0.5_{-1.0}$	$-0.3_{-1.0}$
n	0.4	$0^{+0.5}$	0.4
$\log(\phi_i/\eta)$	$0.5_{-3.2}$	-1.4	$0.5_{-2.9}$
H_0	$68.5^{+1.0}_{-1.4}$	73.0 ± 1.3	70.4 ± 5.5
Ω_{m0}	0.291 ± 0.016	$0.281^{+0.043}_{-0.053}$	0.266 ± 0.046
σ_8			0.862 ± 0.093
S_8			0.802 ± 0.031
DIC	8.53 ± 0.12	703.54 ± 0.33	260.86 ± 0.72
WAIC	8.26 ± 0.21	703.40 ± 0.45	262.36 ± 0.68
$-\ln B$	8.33 ± 0.26	703.56 ± 0.11	262.26 ± 0.29
ΔDIC	0.08 ± 0.14	0.17 ± 0.34	0.2 ± 1.1
ΔWAIC	-0.24 ± 0.27	0.09 ± 0.46	-0.27 ± 0.69
$-\Delta \ln B$	-0.53 ± 0.48	0.07 ± 0.17	-0.10 ± 0.98
Tension against	CMB	CMB + BAO	CMB + BAO + SNe + low-z
R	1.2 ± 2.8	6.3 ± 2.8	1.5 ± 2.8
GoF	$2.33 \pm 0.25\sigma$	$4.20 \pm 0.23\sigma$	$2.93 \pm 0.35\sigma$
S	$2.08 \pm 0.41\sigma$	$3.96 \pm 0.26\sigma$	$1.86 \pm 0.47\sigma$
ΔR	1.2 ± 3.1	-1.2 ± 3.2	3.1 ± 3.5
ΔGoF	$0.39 \pm 0.39\sigma$	$-0.10 \pm 0.30\sigma$	$0.39 \pm 0.46\sigma$
ΔS	$0.40 \pm 0.45\sigma$	$-0.10 \pm 0.31\sigma$	$0.26 \pm 0.48\sigma$

Table 6. Mean and standard deviation of cosmological parameters, late-time observables, and statistical probes for the axion-like dark energy model in section 2. From left to right are datasets of BAO, SNe + low-z, and DES Y1. ΔICs and delta of tension probes are with respect to ΛCDM model presented in table 5. Tension probes of $-\ln R$, GoF and S are with respect to axion-like dark energy model inside table 4 according to "Tension against" row. For parameters not following Gaussian distribution we provide the median and 68% lower and upper bounds (if valid) instead, with colour coding for how heavy the tail is (red for short tail, black for Gaussian, blue for exponential, and cyan for long tail.) If the distribution is clearly single-sided we report the modal and the single-sided 68% bound instead.

H.-W. Chiang, C.G. Boiza and M.B.-L.: arxiv:2503.04898 (JCAP)

Observables-1-

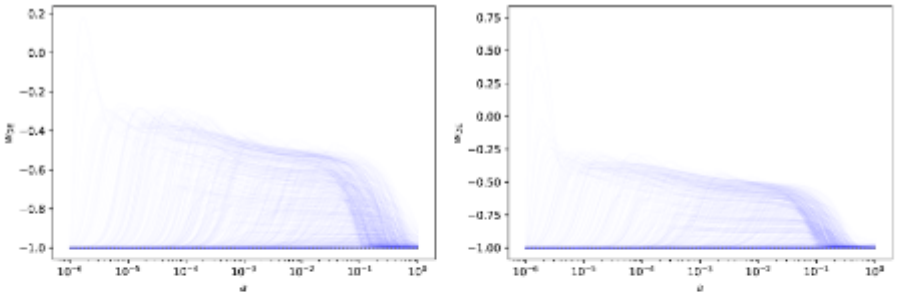

(a) CMB: $w_\phi(a/a_0)$

(b) CMB + BAO: $w_\phi(a/a_0)$

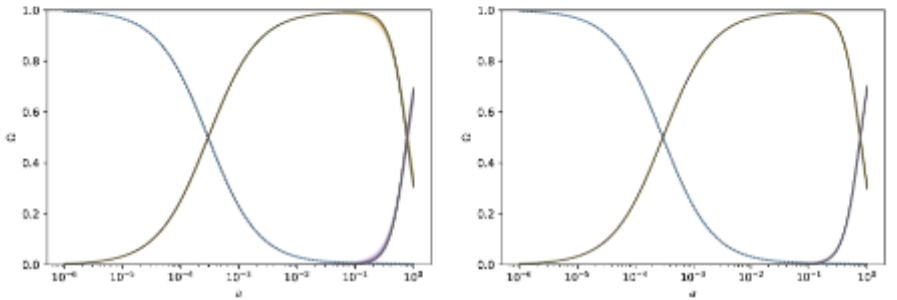

(c) CMB: Ω_r (blue), Ω_n (yellow), Ω_ϕ (purple)

(d) CMB + BAO: Ω_r (blue), Ω_m (yellow), Ω_ϕ (purple)

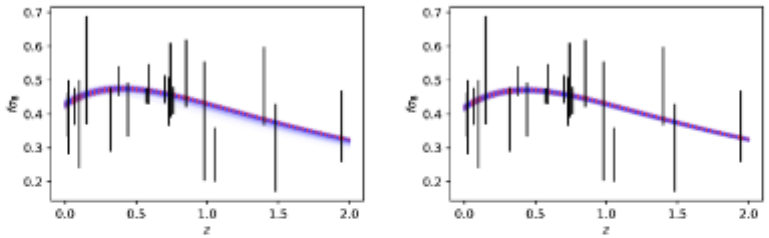

(e) CMB: $f\sigma_8$

(f) CMB + BAO: $f\sigma_8$

Figure 8. The dark energy equation of state w_ϕ (*top*), density parameters (*centre*) of radiation Ω_r (blue), matter Ω_m (yellow) and dark energy Ω_ϕ (purple) as functions of a/a_0, and $f\sigma_8$ (*bottom*) as functions of z for 600 samples drawn from individual fits. *Left* figures: Models fitted against CMB dataset. *Right* figures: Models fitted against CMB + BAO dataset. *Black* line denotes ΛCDM model and non-black lines denote the axion-like dark energy model. Without additional distance measurement, CMB dataset alone permits variation of the density parameter evolution as depicted in Fig. 2. However, once BAO dataset is included, the density parameters stabilise and the tracking regime has to end before $a/a_0 = 1$. In *bottom* figures, the $f\sigma_8$ data are taken from table 2 of [76].

Observables-2-

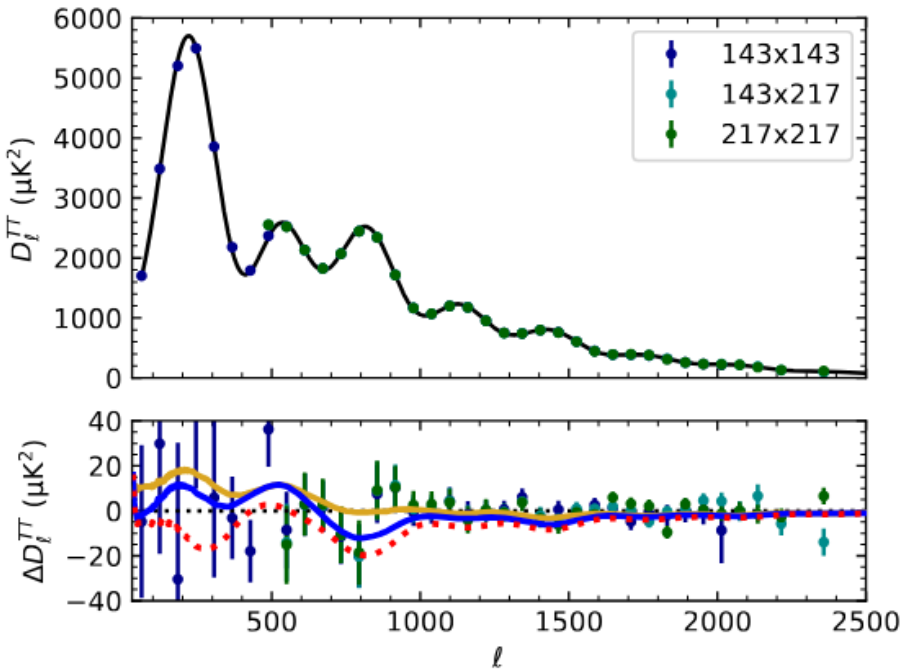

(a) CMB TT power spectrum

Figure 9. The best fit CMB TT power spectrum (*top*) and the residue (*bottom*) against best fit ΛCDM model TT power spectrum of CMB dataset. *Top*: The best fit CMB TT power spectrum of ΛCDM model and the data from Planck CamSpec PR4 data release in Fig. 6 of [16]. *Bottom*: Black *dotted* line and red *dotted* line denote ΛCDM model fitted against CMB and CMB + BAO datasets respectively, and yellow *solid* line and blue *solid* line denotes axion-like dark energy model fitted against CMB and CMB + BAO datasets respectively. There are no visible difference between two models.

Observables-3-

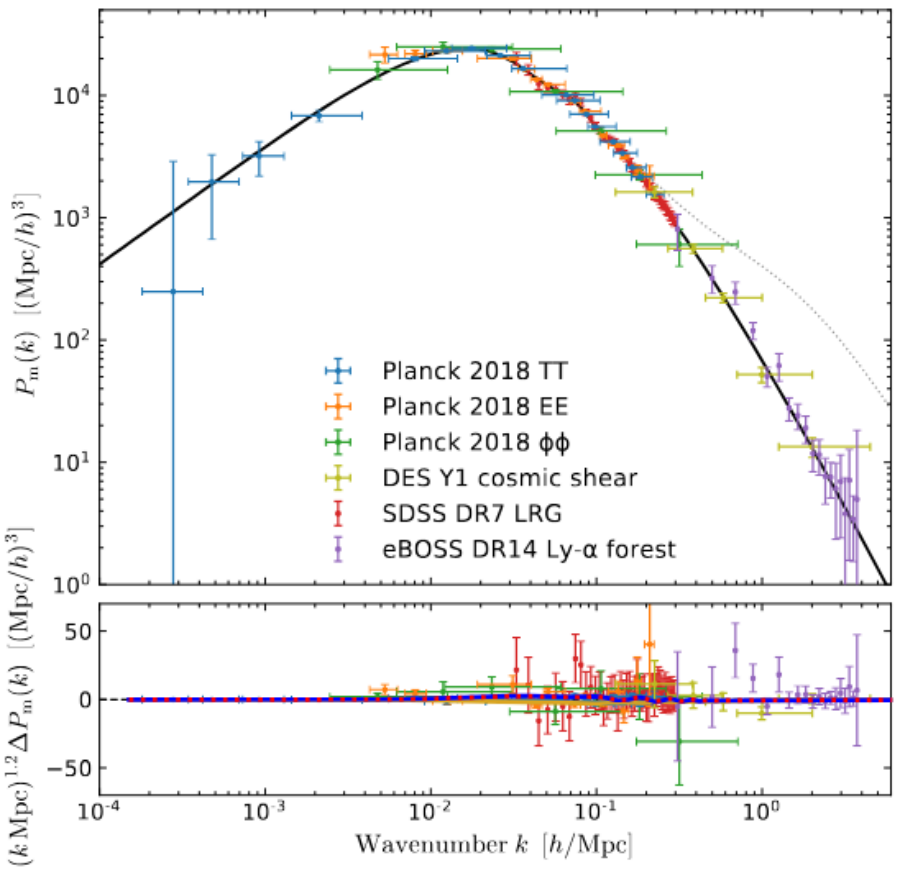

Figure 11. The best fit matter power spectrum (*top*) and the residue (*bottom*) against best fit ΛCDM model matter power spectrum of CMB dataset. *Top*: *Solid* lines represents the linear power spectrum and the *dotted* lines represents the nonlinear power spectrum. Matter power spectrum data taken from Fig. 1 of [79]. *Bottom*: Black *dashed* line and red *dotted* line denote ΛCDM model fitted against CMB and CMB + BAO datasets respectively, and yellow *solid* line and blue *solid* line denotes axion-like dark energy model fitted against CMB and CMB + BAO datasets respectively. There are no visible difference between three best fit models.

Speeding up with fields

Late-time acceleration through a 3-form field

Can we have something beyond scalar fields to describe DE?

- Can we have something beyond scalar fields to describe DE?
  - A possibility come in the form of 3-forms.
  - Inspired in supergravity and string theory: Aurilia, Nicolai, Townsend (1980), Copeland, Lahiri,Wands (1995)
  - Massless 3-form as Cosmological Constant (solving CC problem): Turok, Hawking (1998)
  - Inflation or late time acceleration driven by self-interacting 3-forms: Koivisto, Nunes (2009) and (2010)
  - Non-Gaussianity: Kumar, Mulryne, Nunes, Marto, Moniz (2016)
  - Quantum cosmology with 3-forms: Bouhmadi-López, Brizuela, Garay (2018)
  - DE models (quintessence like and phantom as well): Morais, Bouhmadi-López, Kumar, Marto, Tavakoli, Phys. Dark Univ., arXiv: 1608.01679 , Bouhmadi-López, Marto, Morais and Silva, JCAP, arXiv: 1611.03100 M.B.-L, H.-W. Chiang, C.G. Boiza and P. Chen: arXiv: 2512.09991 (JCAP) and M.B.-L, H.-W. Chiang, C.G. Boiza, J. Ortega del Rio, T. Broadhust and P. Chen: arXiv:2606.27436 (the observational fits)

What are p-forms?

A p-form is a totally anti-symmetric covariant tensor:

$$\omega_{\mu_1 \ldots \mu_p} = \omega_{[\mu_! \ldots \mu_p]} \, .$$

In D-dimensions, the number of degrees of freedom of a massive p-form is

$$\text{degrees of freedom} = \frac{(D-1)!}{(D-1-p)!p!} \, .$$

C. Germani and A. Kehagias, J. Cosmol. Astropart. Phys. 2009, 28 (2009)
Part of the section is based on Morais, B.L, Kumar, Marto and Tavakoli, Phys. Dark Univ. 15, 7 (2017) [arXiv:1608.01679 [gr-qc]]

p-forms in Cosmology

In a 4-dimensional space-time:

- $p = 0$ (scalar field) $\Rightarrow$ 1 degree of freedom
- $p = 1$ (vector field) $\Rightarrow$ 3 degrees of freedom
- $p = 2 \Rightarrow$ 3 degrees of freedom
- $p = 3 \Rightarrow$ 1 degree of freedom

$\Rightarrow$ The scalar field and the 3-form are the only ones compatible with a homogeneous and isotropic universe (in an easy way).

C. Germani and A. Kehagias, J. Cosmol. Astropart. Phys. 2009, 28 (2009)
T. S. Koivisto, D. F. Mota, and C. Pitrou, J. High Energy Phys. 2009, 92 (2009)

The 3-form action

- We will consider the following action for a massive 3-form, $A_{\mu\nu\rho}$, minimally coupled to gravity

$$S^A = \int \mathrm{d}^4\mathbf{x}\sqrt{|\det g_{\mu\nu}|}\left[-\frac{1}{48}F^{\mu\nu\rho\sigma}F_{\mu\nu\rho\sigma} - V\left(A^{\mu\nu\rho}A_{\mu\nu\rho}\right)\right] .$$

- The strength tensor, a 4-form, is defined through the exterior derivative: $F_{\mu\nu\rho\sigma} \equiv 4\nabla_{[\mu}A_{\nu\rho\sigma]}$
- The equation of motion, obtained from variation of S^A, is

$$\nabla_\sigma F^\sigma{}_{\mu\nu\rho} - 12\frac{\partial V}{\partial\left(A^2\right)}A_{\mu\nu\rho} = 0$$

- $\Rightarrow$ a massless 3-form is equivalent to a cosmological constanst

C. Germani and A. Kehagias, J. Cosmol. Astropart. Phys. 2009, 28 (2009)
T. S. Koivisto, D. F. Mota, and C. Pitrou, J. High Energy Phys. 2009, 92 (2009)
M. Duff and P. Van Nieuwenhuizen, Phys. Lett. B 94, 179 (1980)

3-form Cosmology

We consider a homogeneous and isotropic universe described by the Friedmann-Lemaître-Robertson-Walker line element

$$ds^2 = -dt^2 + a^2(t)\gamma_{ij}dx^i dx^j \,.$$

t - cosmic time, $\dot{\{\}} = d\{\}/dt$
a - scale factor
x^i - comoving spatial coordinates (roman indices run from 1 to 3).

Only the purely spatial components of the 3-form are dynamical:

$$A_{0ij} = 0\,, \qquad A_{ijk} = a^3(t)\chi(t)\epsilon_{ijk}\,.$$

T. S. Koivisto, D. F. Mota, and C. Pitrou, J. High Energy Phys. 2009, 92 (2009)
Koivisto and Nunes PLB [arXiv:0907.3883], idem PRD [arXiv:0908.0920]

3-form Cosmology: background equations

$\Rightarrow$ Friedmann Equation

$$3H^2 = \kappa^2 \rho_\chi = \kappa^2 \left[\frac{1}{2} \left(\dot{\chi} + 3H\chi \right)^2 + V(\chi^2) \right] .$$

$\Rightarrow$ Raychaudhuri equation

$$\dot{H} = -\frac{\kappa^2}{2} \left(\rho_\chi + P_\chi \right) = -\frac{\kappa^2}{2} \chi \frac{\partial V}{\partial \chi} .$$

A 3-form can show phantom-like behavior if $\partial V / \partial \chi^2 < 0$.

$\Rightarrow$ Equation of motion

$$\ddot{\chi} + 3H\dot{\chi} + 3\dot{H}\chi + \frac{\partial V}{\partial \chi} = 0 .$$

3-form Cosmology: evolution of χ-1-

Combining the Raychaudhuri equation and the equation of motion for χ:

$$\ddot{\chi} + 3H\dot{\chi} + \left(1 - \frac{\chi^2}{\chi_c^2}\right)\frac{\partial V}{\partial \chi} = 0\,.$$

The static solutions are:

- the critical points of the potential: $\dfrac{\partial V}{\partial \chi} = 0$,
- the limiting points: $\chi = \pm\chi_c$.

Once inside the interval $[-\chi_c, \chi_c]$, the field χ evolves towards a local minimum of V.

3-form Cosmology: evolution of χ-2-

- Independently of the shape of a regular potential, in absence of DM interaction, the 3-form decays rapidly towards the interval $[-\chi_c, \chi_c]$ Koivisto and Nunes PLB [arXiv:0907.3883], idem PRD [arXiv:0908.0920]

- In an expanding Universe, once inside the interval $[-\chi_c, \chi_c]$, the 3-form will end up in one of the minima of the potential (notice $V_{\rm eff} \neq V$).

- If the 3-form stops at the limits of this interval:

$$\chi = \pm\chi_c \quad \text{and} \quad \dot{\chi} = 0$$

- $\longrightarrow$ Universe heads towards a LSBR event $(\chi_c = \sqrt{2/3\kappa^2})$

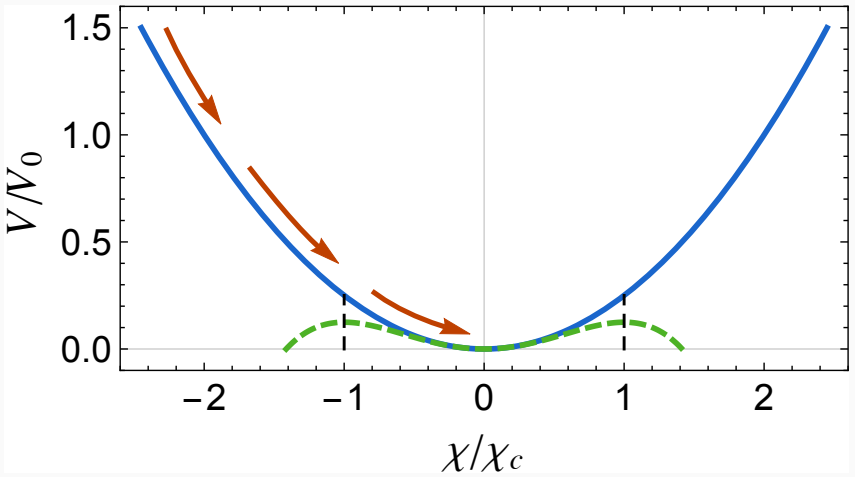

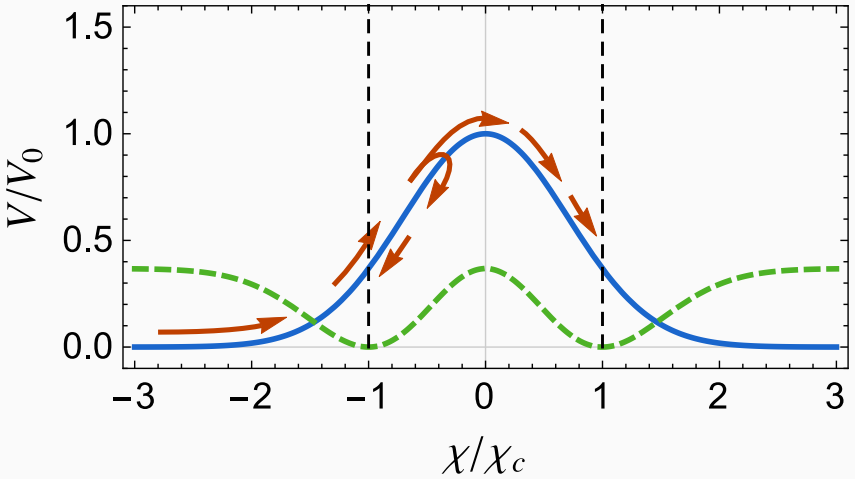

3-forms & with a Gaussian potential: a dynamical system approach

Using a Dynamical Systems representation Morais *et al* PofDU [arxiv:1608.01679]; BL *et al*, JCAP [arXiv:1611.03100]

$$u = (\pi/2)\arctan(\chi/\chi_c) \qquad y = (\dot{\chi} + 3H\chi)/(3H\chi_c) \qquad z = \sqrt{\kappa^2 V/3H^2}$$

- Three **matter era** points:
  two repulsive - $(\pm 1, 0, 0)$
  one saddle - $(0, 0, 0)$
- One potential dom. **de Sitter** point: saddle - $(0, 0, 1)$
- Two **LSBR event** points:
  attractor - $(\pm 1/2, \pm 1, 0)$
- Four **unphysical** points:
  saddles - $(\pm 1, \pm 1, 0)$

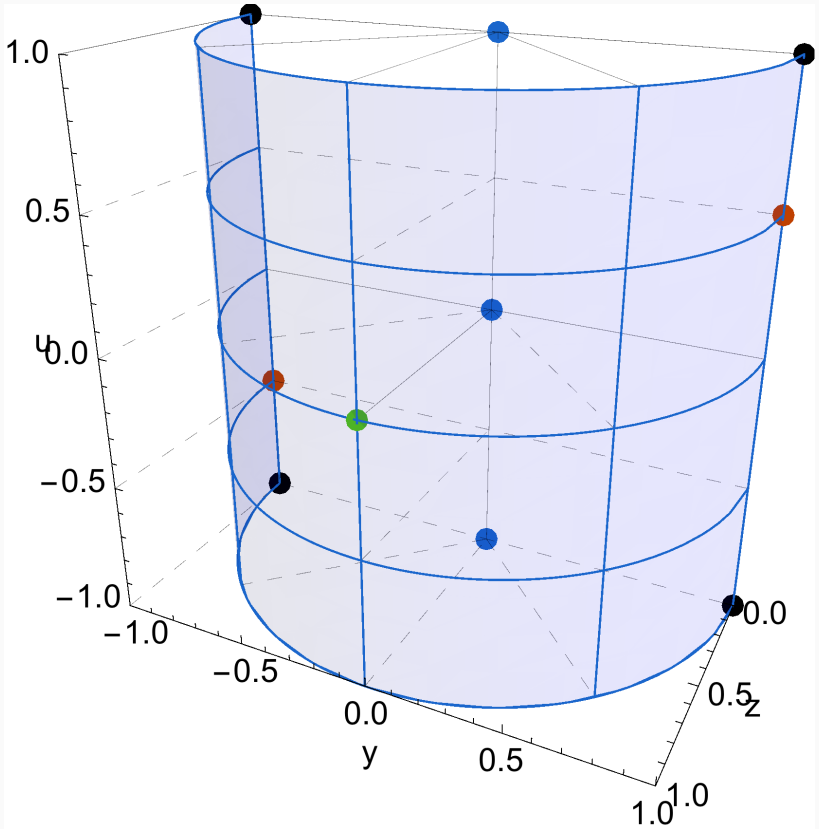

Fixed points in the non-interacting case

Fitting the model with a Gaussian potential-1-

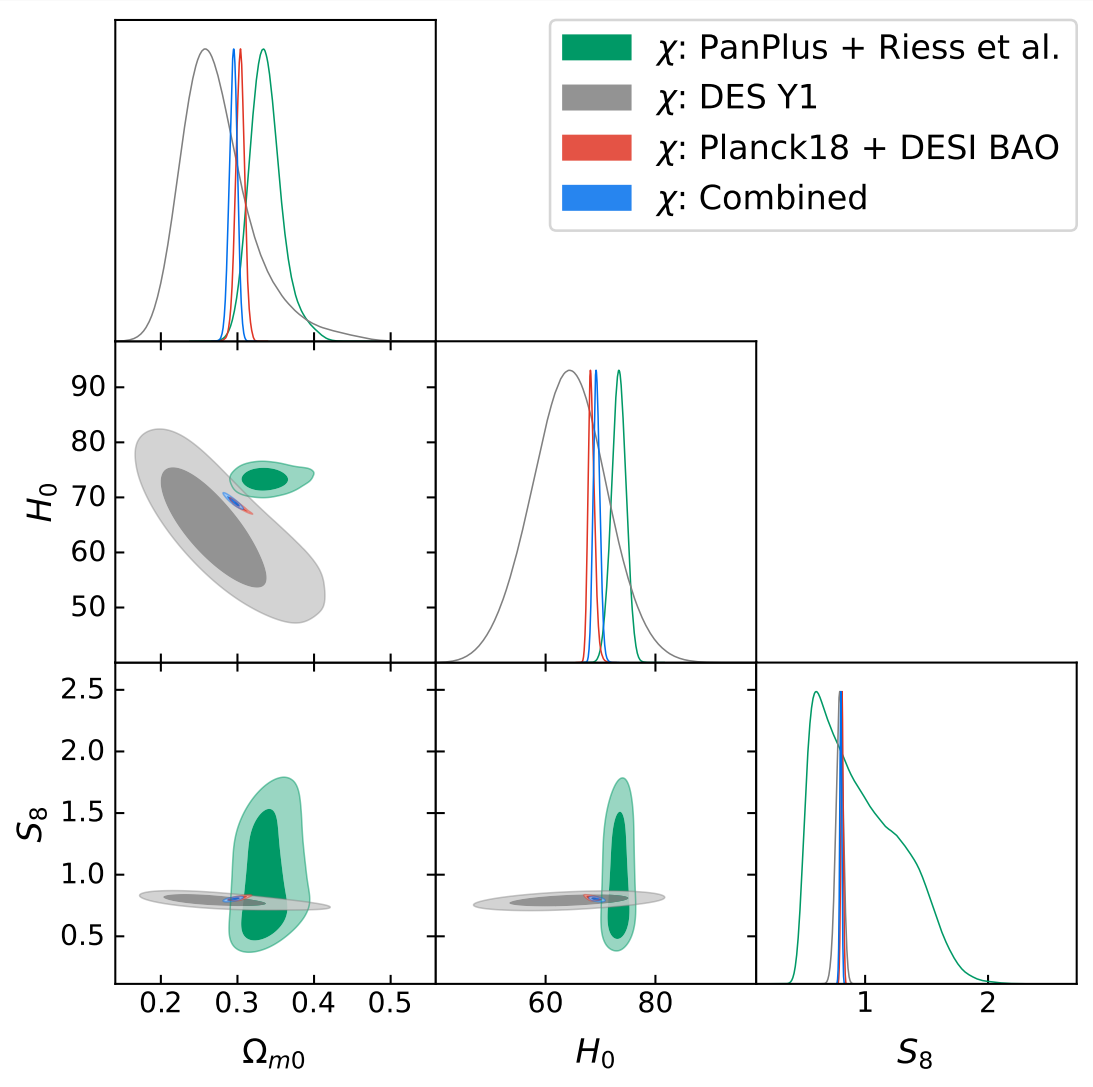

M.B.-L, C.G. Boiza, H.-W. Chiang and P. Chen: arXiv: 2512.09991 (JCAP)

Comparing the model to LCDM

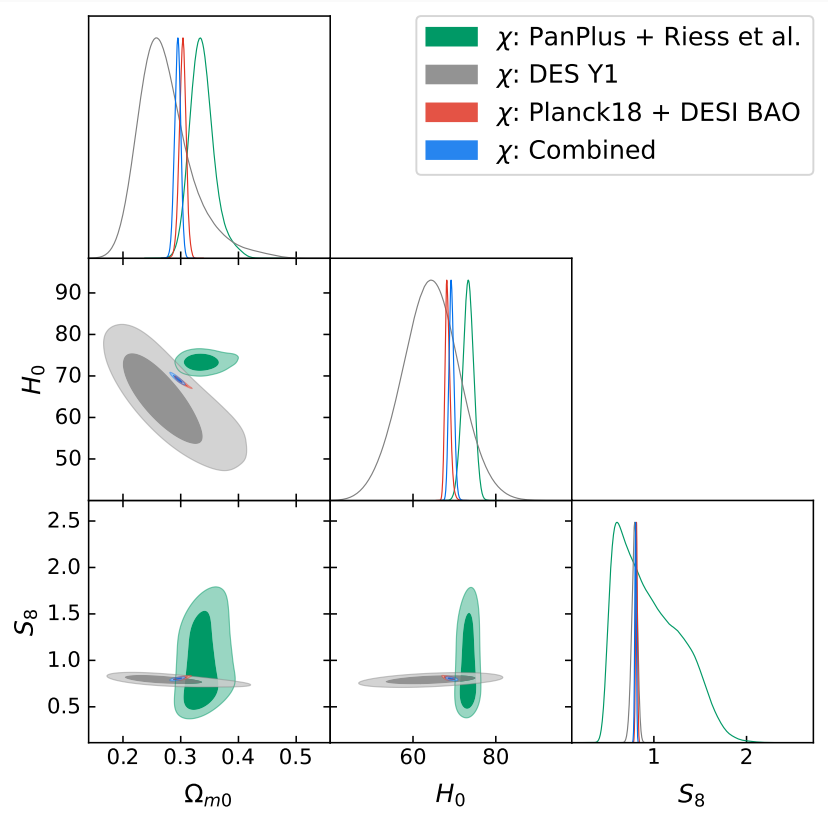

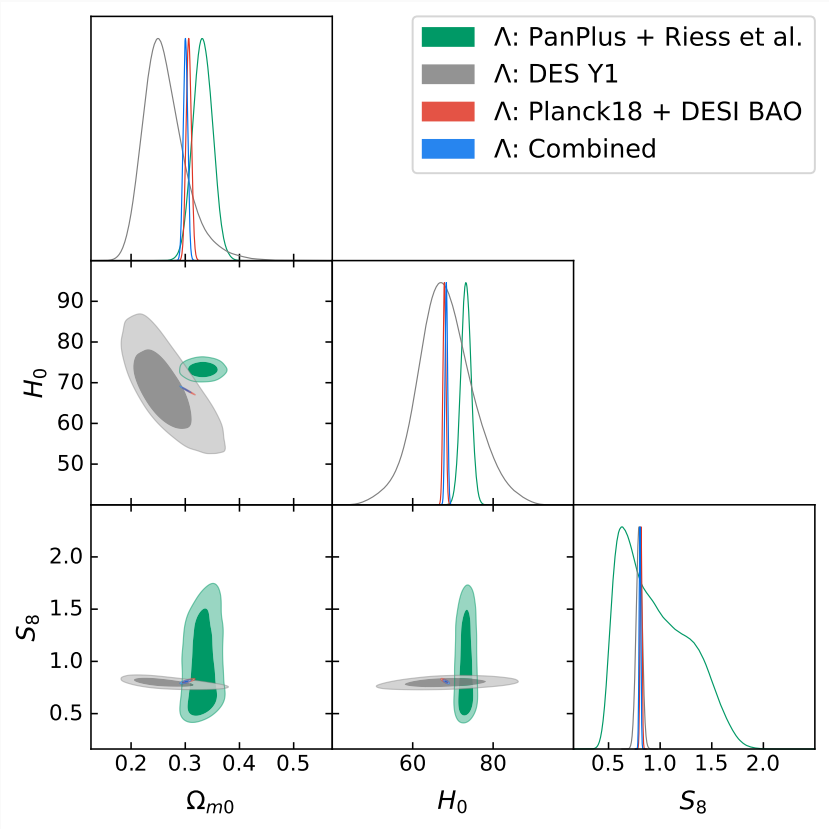

M.B.-L, C.G. Boiza, H.-W. Chiang and P. Chen: arXiv: 2512.09991 (JCAP)

Fitting the model with a Gaussian potential-2-

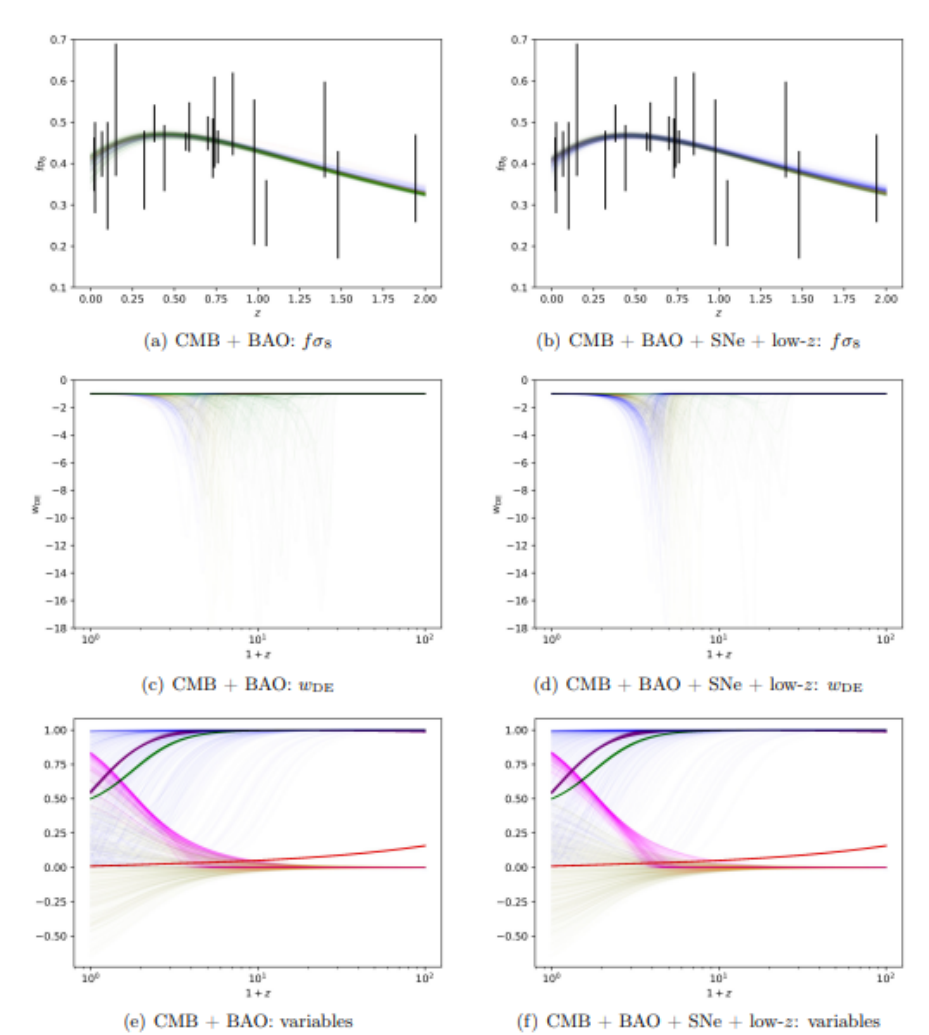

(a) CMB + BAO: $f\sigma_8$ (b) CMB + BAO + SNe + low-z: $f\sigma_8$

(c) CMB + BAO: $w_{\rm DE}$ (d) CMB + BAO + SNe + low-z: $w_{\rm DE}$

(e) CMB + BAO: variables (f) CMB + BAO + SNe + low-z: variables

Figure 5. $f\sigma_8$ (*top*), dark energy EoS $w_{\rm DE}$ (*centre*) and dynamical variables (*bottom*) as functions of z for 600 samples drawn from individual fits, against CMB + BAO (*left*) and CMB + BAO + SNe + low-z (*right*) dataset. In *bottom* figures, colour represents variables of section 3.2: blue: v, purple: s, green: $\mathfrak{h}$, red: r, yellow: y, magemta: $\kappa\sqrt{V/3}/H$. In *top* and *centre* figures, the colour indicates the initial field strength $\log_{10}(a_i^3\sqrt{\xi}\kappa\chi_i)$: (red: $> -3/4$, blue: $-3/4 \sim -5/4$, yellow: $-5/4 \sim -7/4$, green: $< -7/4$). In *top* figures, the $f\sigma_8$ data are taken from table 2 of [119].

M.B.-L, C.G. Boiza, H.-W. Chiang and P. Chen: arXiv: 2512.09991 (JCAP)

Fitting the model with a Gaussian potential-3-

	CMB	Left + BAO	Left + SNe	Left + low-z	Left + DES Y1
$10^3\Omega_{b0}h^2$	22.19 ± 0.13	22.29 ± 0.12	22.26 ± 0.12	22.34 ± 0.12	22.38 ± 0.12
$10^3\Omega_{c0}h^2$	119.7 ± 1.0	118.26 ± 0.81	118.56 ± 0.79	117.80 ± 0.76	117.27 ± 0.72
$10^5\theta_{\rm MC}$	1040.77 ± 0.25	1040.94 ± 0.24	1040.91 ± 0.24	1041.01 ± 0.24	1041.05 ± 0.24
$\ln(10^{10}A_s)$	3.037 ± 0.014	3.044 ± 0.014	3.043 ± 0.014	3.047 ± 0.014	3.046 ± 0.014
n_s	0.9636 ± 0.0040	0.9672 ± 0.0036	0.9665 ± 0.0036	0.9685 ± 0.0036	0.9693 ± 0.0036
$\tau_{\rm reio}$	0.0524 ± 0.0071	0.0571 ± 0.0071	0.0562 ± 0.0070	0.0587 ± 0.0071	0.0589 ± 0.0071
H_0	67.24 ± 0.46	67.89 ± 0.36	67.76 ± 0.35	68.12 ± 0.34	68.36 ± 0.32
Ω_{m0}	0.3154 ± 0.0064	0.3064 ± 0.0048	0.3082 ± 0.0047	0.3034 ± 0.0044	0.3003 ± 0.0042
σ_8	0.8077 ± 0.0055	0.8064 ± 0.0056	0.8067 ± 0.0056	0.8061 ± 0.0057	0.8041 ± 0.0055
S_8	0.828 ± 0.011	0.8149 ± 0.0090	0.8176 ± 0.0090	0.8107 ± 0.0087	0.8044 ± 0.0080
DIC	5497.90 ± 0.12	5507.21 ± 0.37	6209.34 ± 0.14	6217.77 ± 0.43	6477.38 ± 0.28
WAIC	5499.09 ± 0.50	5507.85 ± 0.18	6210.36 ± 0.21	6218.68 ± 0.21	6481.16 ± 0.22
$-\ln B$	5499.3 ± 1.1	5508.13 ± 0.73	6210.51 ± 0.44	6219.1 ± 1.4	6479.9 ± 1.2

Table 3. Mean and standard deviation of cosmological parameters, late-time observables, and statistical probes for ΛCDM model. From left to right are gradually larger datasets that progressively add in datasets of CMB, BAO, etc., as defined in section 4.1.

	CMB	Left + BAO	Left + SNe	Left + low-z	Left + DES Y1
$10^3\Omega_{b0}h^2$	22.19 ± 0.13	22.25 ± 0.13	22.23 ± 0.12	22.26 ± 0.13	22.30 ± 0.13
$10^3\Omega_{c0}h^2$	119.6 ± 1.1	118.79 ± 0.95	118.89 ± 0.86	118.79 ± 0.98	118.3 ± 1.0
$10^5\theta_{\rm MC}$	1040.78 ± 0.26	1040.88 ± 0.25	1040.88 ± 0.24	1040.88 ± 0.26	1040.93 ± 0.24
$\ln(10^{10}A_s)$	3.037 ± 0.014	3.041 ± 0.014	3.040 ± 0.014	3.039 ± 0.015	3.038 ± 0.015
n_s	0.9640 ± 0.0040	0.9662 ± 0.0037	0.9658 ± 0.0037	0.9663 ± 0.0038	0.9670 ± 0.0039
$\tau_{\rm reio}$	0.0523 ± 0.0070	0.0550 ± 0.0073	0.0547 ± 0.0072	0.0543 ± 0.0077	0.0540 ± 0.0077
$\log_{10}\xi$	-3.2	-3.2	-3.4	-3.4	-3.4
$({\rm KE}_i + V_*)/\rho_{\rm DE,0}$	1.0000 ± 0.0021	1.0002 ± 0.0027	1.0000 ± 0.0017	1.0004 ± 0.0020	1.0006 ± 0.0038
$\log_{10}(a_i^3\sqrt{\xi}\kappa\chi_i)$	$-2.3^{+0.6}$	$-1.6^{+0.3}$	$-1.86^{+0.69}_{-0.59}$	$-1.27^{+0.28}_{-0.21}$	$-1.23^{+0.27}_{-0.23}$
$(\dot\chi_i + 3H_i\chi_i)\rho_{\rm DE,0}^{-1/2}$	0.02 ± 0.51	0.02 ± 0.51	-0.03 ± 0.48	-0.06 ± 0.46	-0.08 ± 0.45
H_0	$67.57^{+0.58}_{-0.75}$	$68.29^{+0.56}_{-0.61}$	$68.02^{+0.45}_{-0.46}$	68.92 ± 0.59	69.21 ± 0.60
Ω_{m0}	$0.3116^{+0.0090}_{-0.0075}$	0.3030 ± 0.0060	0.3062 ± 0.0051	0.2984 ± 0.0052	0.2950 ± 0.0053
σ_8	$0.8076^{+0.0060}_{-0.0063}$	0.8080 ± 0.0070	0.8069 ± 0.0065	0.8101 ± 0.0069	0.8083 ± 0.0066
S_8	$0.822^{+0.013}_{-0.011}$	0.8119 ± 0.0094	0.8151 ± 0.0091	0.8079 ± 0.0086	0.8015 ± 0.0085
DIC	5498.72 ± 0.01	5507.62 ± 0.54	6209.59 ± 0.53	6216.09 ± 0.31	6476.4 ± 1.2
WAIC	5499.58 ± 0.21	5508.21 ± 0.29	6210.14 ± 0.45	6217.51 ± 0.65	6479.94 ± 0.06
$-\ln B$	5500.0 ± 1.1	5508.5 ± 1.2	6210.04 ± 0.77	6216.24 ± 0.20	6475.82 ± 0.11
ΔDIC	0.82 ± 0.15	0.40 ± 0.44	0.25 ± 0.56	-1.68 ± 0.60	-1.0 ± 1.3
ΔWAIC	0.49 ± 0.63	0.36 ± 0.36	-0.22 ± 0.52	-1.17 ± 0.70	-1.22 ± 0.27
$-\Delta\ln B$	0.8 ± 1.7	0.3 ± 1.5	-0.47 ± 0.94	-2.9 ± 1.7	-4.1 ± 1.4

Table 4. Mean and standard deviation of cosmological parameters, late-time observables, and statistical probes for the 3-form dark energy model in section 2. From left to right are gradually larger datasets of CMB, CMB + BAO, CMB + BAO + SNe, etc., as defined in section 4.1. ΔICs are with respect to ΛCDM model presented in table 3. For parameters not following Gaussian distribution we provide the median and 68% lower and upper bounds (if valid) instead, with color coding for how heavy the tail is (red for short tail, black for Gaussian, blue for exponential, and cyan for long tail.) For single-sided distributions we report the modal and the single-sided 68% bound instead.

Fitting the model with a Gaussian potential-4-

	BAO	SNe + low-z	DES Y1
$10^3\Omega_{c0}h^2$	116.7 ± 8.3	155 ± 11	86^{+23}_{-10}
$10^5\theta_{\rm MC}$	1042 ± 10	1090 ± 11	1005^{+45}_{-34}
$\ln(10^{10}A_s)$			$3.41^{+0.30}_{-0.26}$
H_0	68.71 ± 0.80	73.2 ± 1.3	65.9 ± 7.1
Ω_{m0}	0.295 ± 0.015	0.332 ± 0.018	$0.250^{+0.040}_{-0.032}$
σ_8			0.845 ± 0.086
S_8			0.791 ± 0.029
DIC	8.45 ± 0.05	703.37 ± 0.03	260.64 ± 0.75
WAIC	8.51 ± 0.15	703.31 ± 0.03	262.63 ± 0.10
$-\ln B$	8.86 ± 0.34	703.49 ± 0.11	262.35 ± 0.87
Tension against	CMB	CMB + BAO	CMB + BAO + SNe + low-z
$-\ln R$	0.0 ± 1.4	7.5 ± 1.6	-1.6 ± 2.1
GoF	$1.94 \pm 0.30\sigma$	$4.30 \pm 0.20\sigma$	$2.54 \pm 0.30\sigma$
S	$1.68 \pm 0.18\sigma$	$4.06 \pm 0.17\sigma$	$1.60 \pm 0.07\sigma$

Table 5. Mean and standard deviation of cosmological parameters, late-time observables, and statistical probes for ΛCDM model. From left to right are datasets of BAO, SNe + low-z, and DES Y1. Tension probes of $-\ln R$, GoF and S are with respect to ΛCDM model inside table 3 according to "Tension against" row. For parameters not following Gaussian distribution we provide the median and 68% lower and upper bounds (if valid) instead, with colour coding for how heavy the tail is (red for short tail, black for Gaussian, blue for exponential, and cyan for long tail.)

M.B.-L, C.G. Boiza, H.-W. Chiang and P. Chen: arXiv: 2512.09991 (JCAP)

Smooth and non-smooth sign-switching dark energy models

Motivation

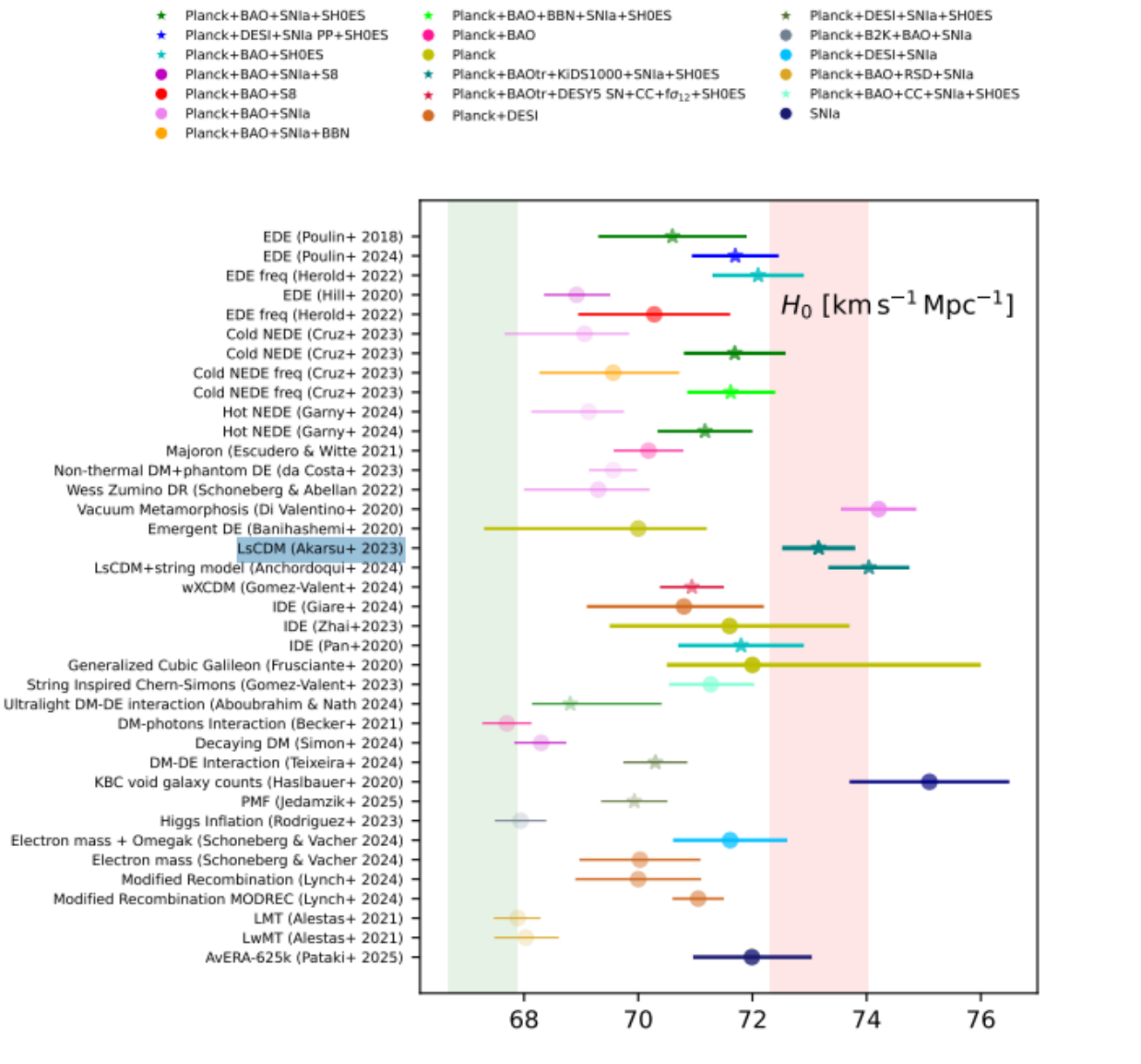

E. Di Valentino et al. [arXiv:2504.01669 [astro-ph.CO]]

Theoretical model

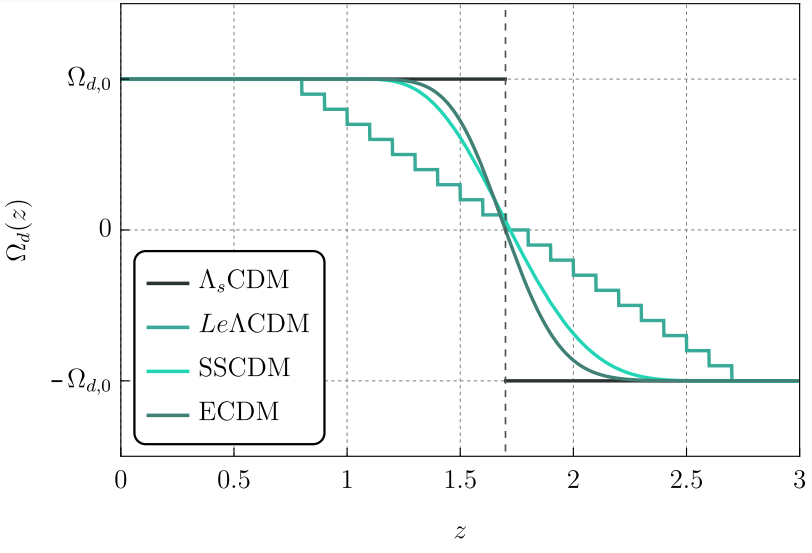

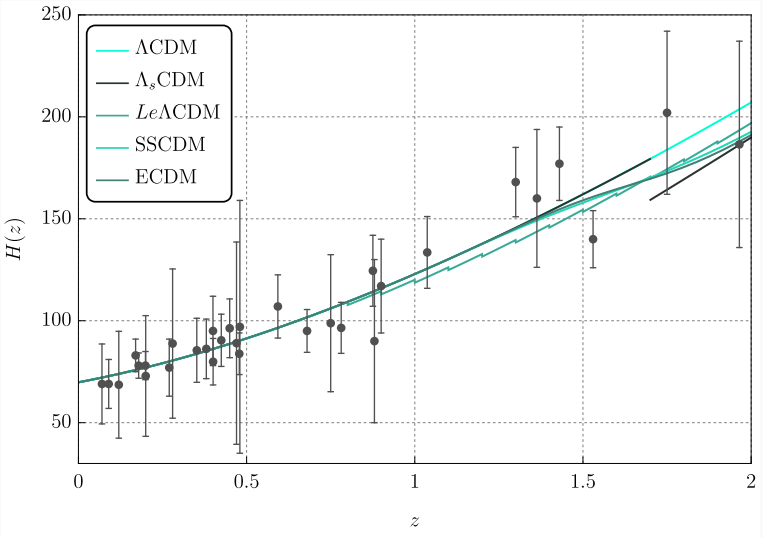

O. Akarsu, S. Kumar, E. Özülker, J. A. Vázquez, arXiv:2108.09239 (PRD).

M.B.-L. and B. Ibarra-Uriondo arXiv: 2506.12139 (PRD).

Cosmographic parameters

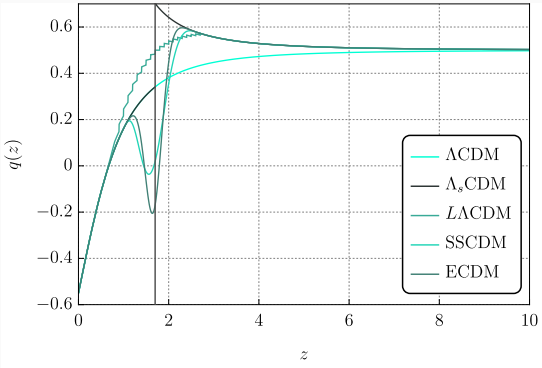

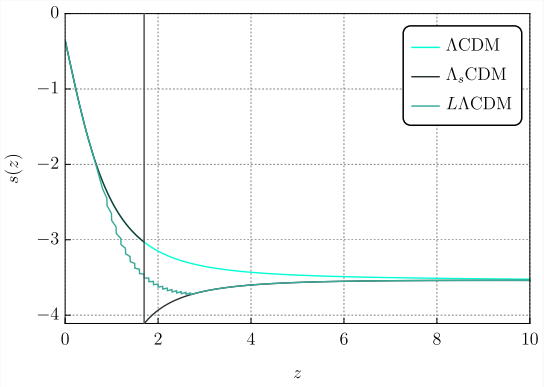

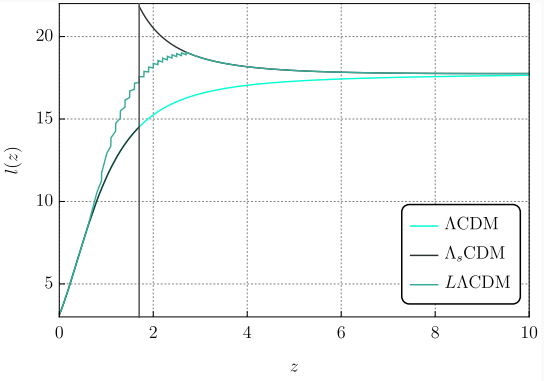

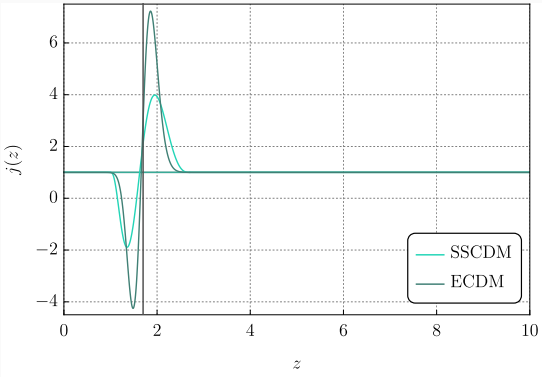

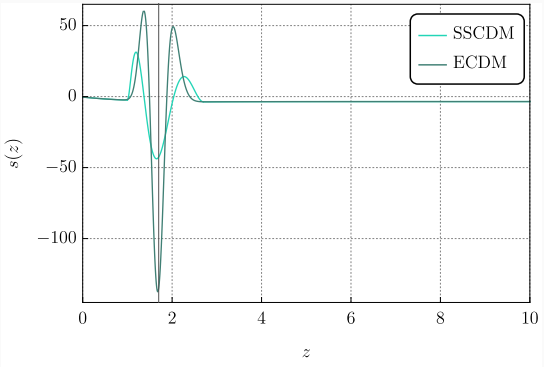

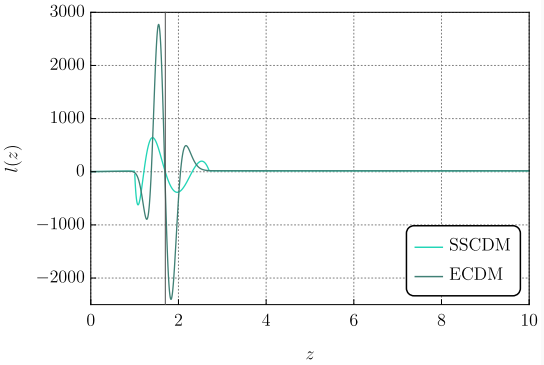

M.B.-L. and B. Ibarra-Uriondo arXiv: 2506.12139 (PRD).

Gravitational potential

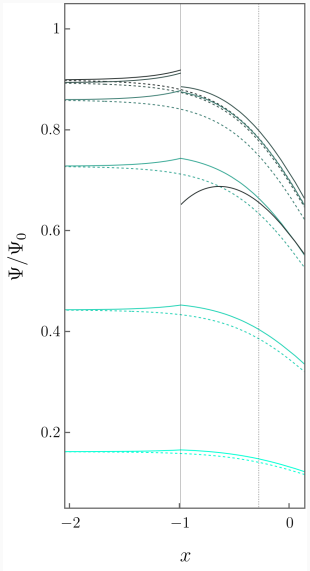

(A) Λ_sCDM

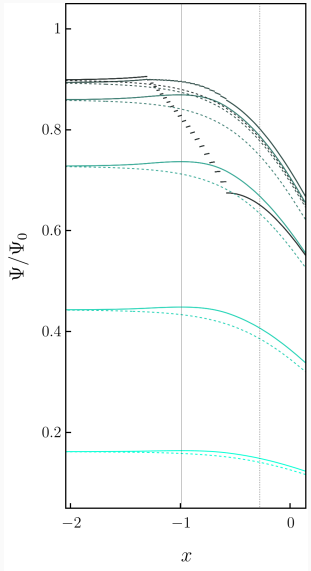

(B) LΛCDM

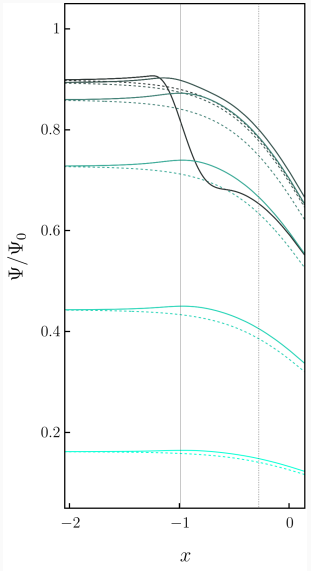

(C) SSCDM

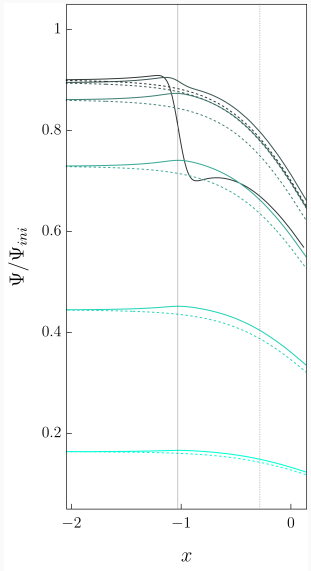

(D) ECDM

Gravitational potential Ψ/Ψ_{ini} for the four models compared with ΛCDM. Modes ranging between $k = 3.33 \times 10^{-4}$h Mpc^{-1} and k = 0.1h Mpc^{-1}. We have set the initial conditions as $\Psi_{\rm ini} = 1$ (which implies $\delta_{\rm ini} = -2$), and subsequently rescale all resulting solutions by the physical value of $\delta_{\rm phys}(k)$.

M.B.-L. and B. Ibarra-Uriondo arXiv: 2506.18992 (Phys. of Dark Universe).

$f\sigma_8$

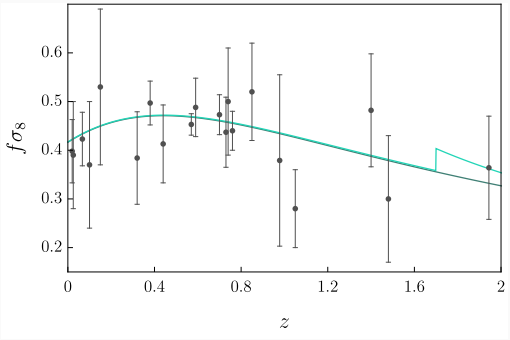

(A) Λ_sCDM

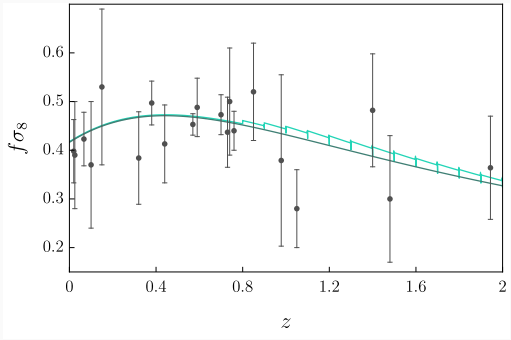

(B) LΛCDM

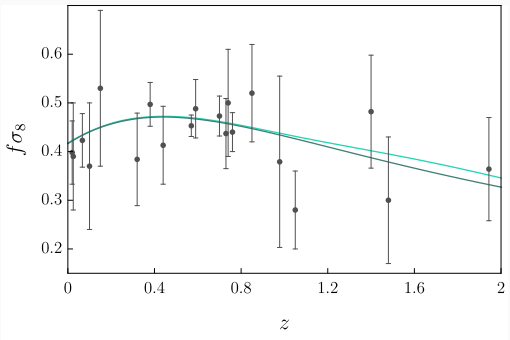

(C) SSCDM

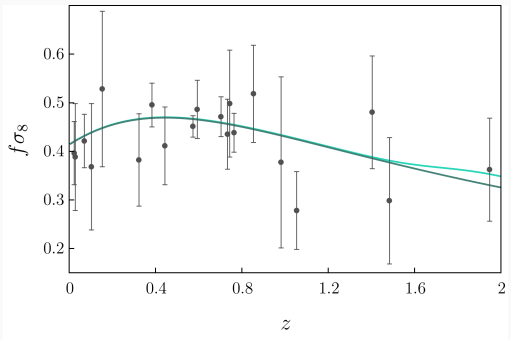

(D) ECDM

Evolution of $f\sigma_8$ for $0 < z < 2$. Light green lines: studied models. Dark green line: ΛCDM.

M.B.-L. and B. Ibarra-Uriondo arXiv: 2506.18992 (Phys. of Dark Universe).

Fitting the model-1-

Model	H_0	Ω_{m0}	$10^2\Omega_{b0}h^2$	$z_\uparrow/z_\downarrow$	$\Delta z/dz/\eta$
			CMB		
ΛCDM	67.33 ± 0.54	0.3156 ± 0.0074	2.2362 ± 0.0141		
Λ_sCDM	$70.06^{+0.25}_{-2.80}$	$0.2928^{+0.0251}_{-0.0059}$	2.2362 ± 0.0135	$> 1.35(95\%CL)$	
LΛCDM	$71.40^{+0.69}_{-4.02}$	$0.2829^{+0.0329}_{-0.0101}$	2.2361 ± 0.0134	$> 1.58(95\%CL)$	$< 0.79(95\%CL)$
SSCDM	$71.32^{+0.53}_{-4.08}$	$0.2837^{+0.0336}_{-0.0090}$	2.2359 ± 0.0135	$> 1.84(95\%CL)$	$< 3.60(95\%CL)$
ECDM	$70.31^{+0.34}_{-3.11}$	$0.2909^{+0.0272}_{-0.0676}$	2.2359 ± 0.0136	$> 1.35(95\%CL)$	unconstrained
			BAO		
ΛCDM	68.75 ± 0.45	0.2973 ± 0.0087	2.2347 ± 0.0364		
Λ_sCDM	68.72 ± 0.43	0.2975 ± 0.0087	2.2322 ± 0.0357	$> 2.41(95\%CL)$	
LΛCDM	69.66 ± 0.78	0.3224 ± 0.0184	2.2326 ± 0.0357	$> 1.56(95\%CL)$	$0.36^{+0.13}_{-0.22}$
SSCDM	69.58 ± 1.04	0.3214 ± 0.0265	2.2322 ± 0.0361	$> 2.77(95\%CL)$	$< 4.11(95\%CL)$
ECDM	$68.94^{+0.37}_{-0.69}$	$0.3035^{+0.0066}_{-0.0155}$	2.2329 ± 0.0356	$> 1.63(95\%CL)$	$> 2.23(95\%CL)$
			SN		
ΛCDM	73.49 ± 1.02	0.3359 ± 0.0190	2.2330 ± 0.0362		
Λ_sCDM	73.52 ± 1.01	0.3336 ± 0.0180	2.2311 ± 0.0360	unconstrained	
LΛCDM	73.51 ± 1.02	0.3385 ± 0.0251	2.2325 ± 0.0351	unconstrained	$< 0.72(95\%CL)$
SSCDM	73.49 ± 1.02	$0.3359^{+0.018}_{0.020}$	2.2324 ± 0.0357	unconstrained	$< 3.58(95\%CL)$
ECDM	73.50 ± 1.00	$0.3347^{+0.0177}_{-0.0198}$	2.2333 ± 0.0359	unconstrained	unconstrained
			CMB + BAO		
ΛCDM	68.41 ± 0.29	0.3009 ± 0.0037	2.2516 ± 0.0122		
Λ_sCDM	68.75 ± 0.33	0.3013 ± 0.0038	2.2402 ± 0.0124	$3.01^{+0.26}_{-0.60}$	
LΛCDM	$68.79^{+0.31}_{-0.35}$	0.3014 ± 0.0038	2.2387 ± 0.0128	$> 2.66(95\%CL)$	$< 0.64(95\%CL)$
SSCDM	68.76 ± 0.32	0.3014 ± 0.0038	2.2399 ± 0.0125	$> 2.79(95\%CL)$	$< 2.66(95\%CL)$
ECDM	68.74 ± 0.32	0.3015 ± 0.0038	2.2401 ± 0.0126	$3.06^{+0.27}_{-0.60}$	$> 3.40(95\%CL)$
			CMB + BAO + SN		
ΛCDM	68.73 ± 0.28	0.2972 ± 0.0035	2.2607 ± 0.0119		
Λ_sCDM	69.12 ± 0.31	0.2980 ± 0.0035	2.2455 ± 0.0124	$2.77^{+0.10}_{-0.44}$	
LΛCDM	$69.28^{+0.33}_{-0.43}$	0.2977 ± 0.0037	2.2406 ± 0.0135	$> 2.59(95\%CL)$	$< 0.737(95\%CL)$
SSCDM	69.12 ± 0.30	0.2980 ± 0.0035	2.2455 ± 0.0123	$3.56^{+0.70}_{-0.52}$	$< 2.80(95\%CL)$
ECDM	$69.14^{+0.30}_{-0.64}$	0.2979 ± 0.0036	2.2450 ± 0.0126	$2.86^{+0.16}_{-0.49}$	$> 1.96(95\%CL)$

Table III: *Mean values and standard deviations of the cosmological parameters obtained for each sign-switching models, and for ΛCDM paradigm, under the five different dataset combinations considered in this work:* ***Combination I*** *(CMB),* ***Combination II*** *(BAO),* ***Combination III*** *(SN),* ***Combination IV*** *(CMB+BAO) and* ***Combination V*** *(CMB+BAO+SN).*

B. Ibarra-Uriondo and M.B.-L. arXiv:2602.12347 (Phys. of Dark Universe)

Fitting the model-2-

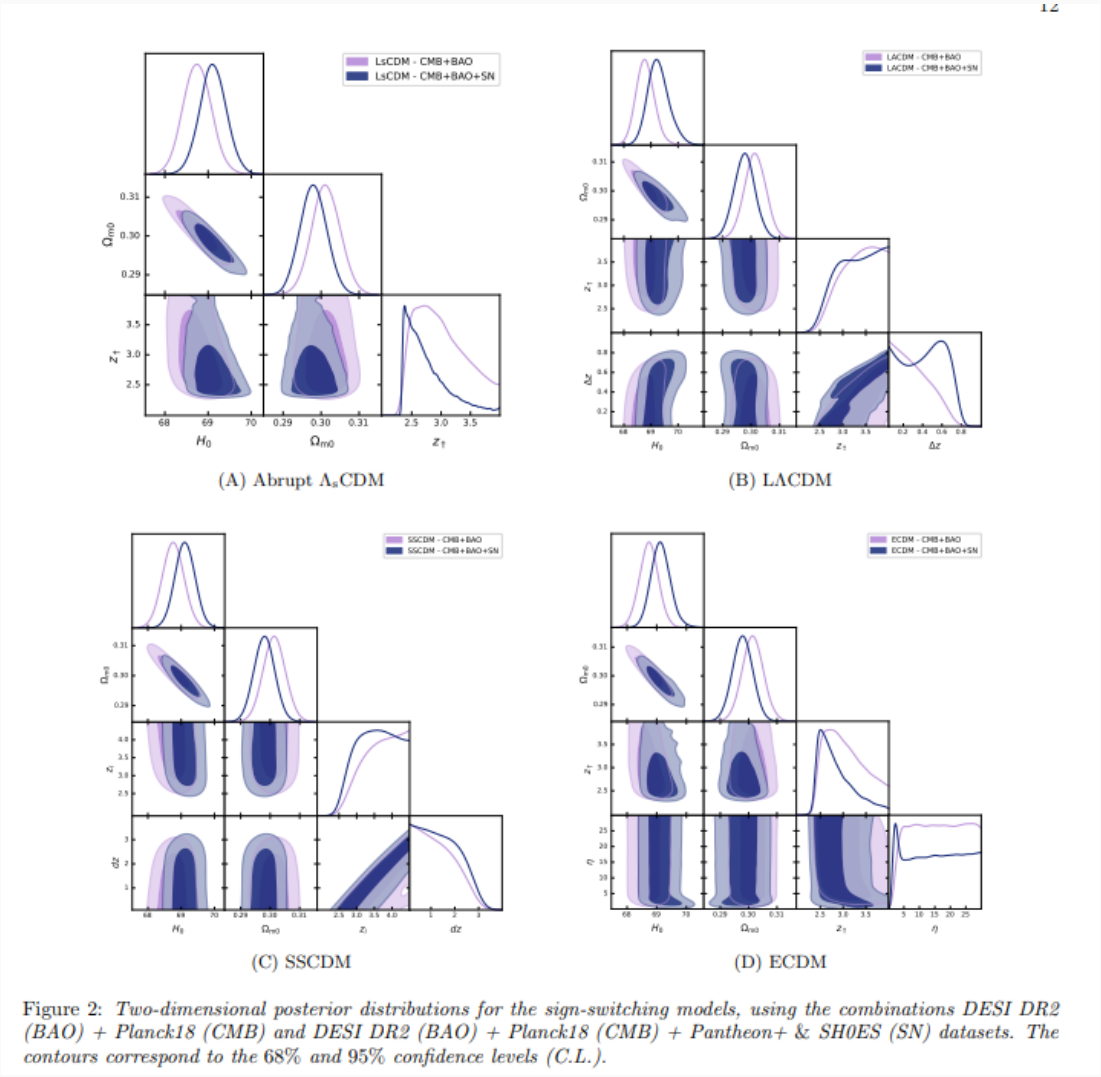

(A) Abrupt Λ_sCDM (B) LACDM

(C) SSCDM (D) ECDM

Figure 2: *Two-dimensional posterior distributions for the sign-switching models, using the combinations DESI DR2 (BAO) + Planck18 (CMB) and DESI DR2 (BAO) + Planck18 (CMB) + Pantheon+ & SH0ES (SN) datasets. The contours correspond to the 68% and 95% confidence levels (C.L.).*

B. Ibarra-Uriondo and M.B.-L. arXiv:2602.12347 (Phys. of Dark Universe)

Fitting the model-3-

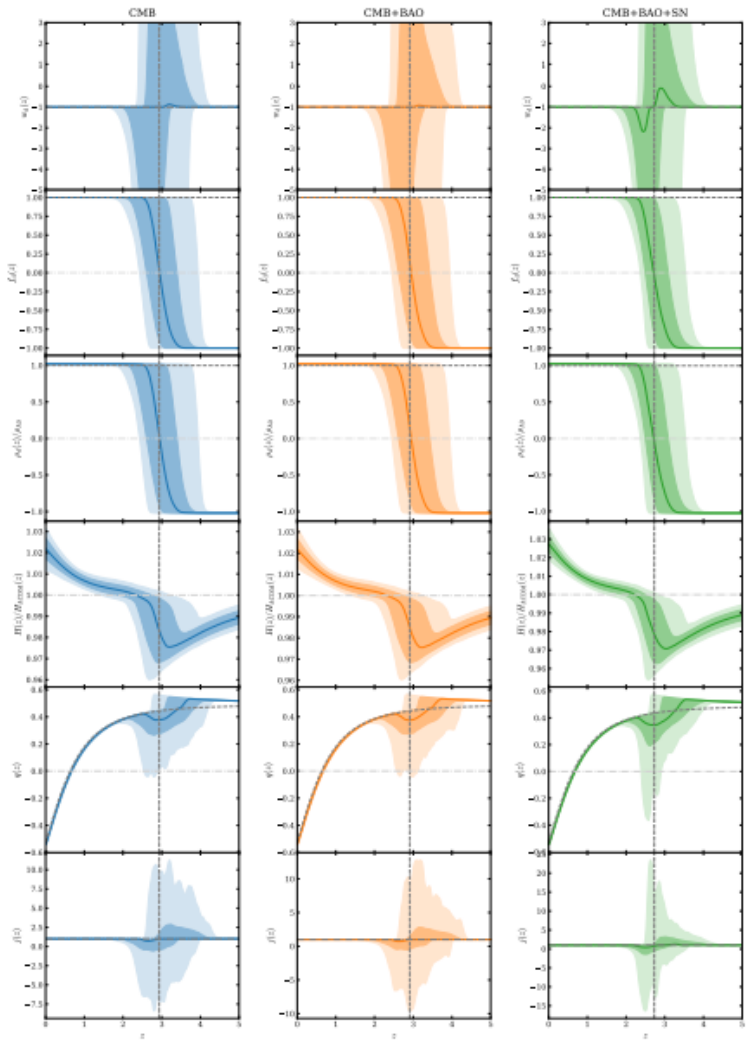

Figure 3: *Reconstructed EoS, energy density normalized to the current value, Hubble parameter, deceleration parameter and jerk for the SSCDM models with Planck18 + DESI DR2 + Pantheon+ & SH0ES (left-most column), and with Planck18 + DESI DR2 (central column) and the Planck18 (right-most column). We also plot the reconstructed Hubble rate and energy density normalized to the Planck PR4 values for ΛCDM, for which* $\Omega_{m0} = 0.315$ *and* $H_0 = 67.26$ *km/s/Mpc [127]. The solid colored lines represent the most-probable value and the shaded regions show the 68% and 95% confidence intervals around it. The grey dashed lines correspond to ΛCDM values. In the plots of* $q(z)$ *we also show in black dash-dotted line the border between deceleration* ($q > 0$) *and acceleration* ($q < 0$) *regimes, i.e.,* $q=0$.

Fitting the model-4-

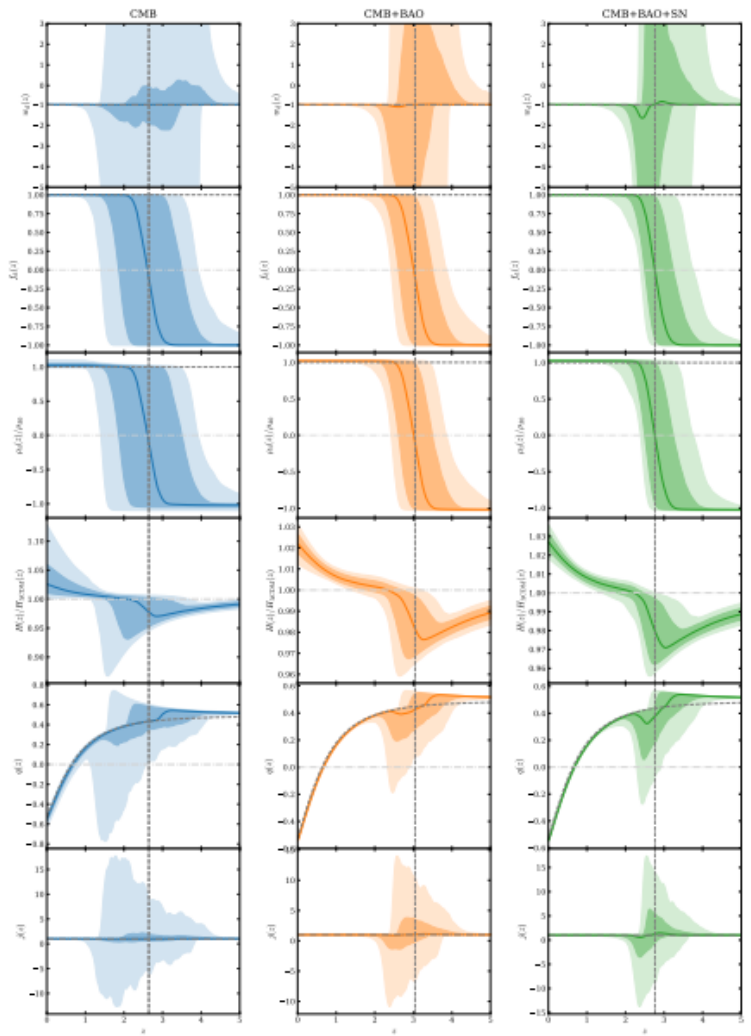

Figure 4: *Reconstructed EoS, energy density normalized to the current value, deceleration parameter and jerk for the ECDM model with Planck18 + DESI DR2 + PantheonPlus & SH0ES (left-most column), and with Planck18 + DESI DR2 (central column) and the Planck18 (right-most column). We also plot the reconstructed Hubble rate and energy density normalized to the Planck PR4 values for ΛCDM, for which $\Omega_{m0} = 0.315$ and $H_0 = 67.26$ km/s/Mpc [114]. The solid colored lines represent the most-probable value and the shaded regions show the 68% and 95% confidence intervals around it. The grey dashed lines correspond to ΛCDM values. In the plots of $q(z)$ we also show in black dash-dotted line the border between deceleration ($q > 0$) and acceleration ($q < 0$) regimes, i.e., $q=0$.*

Conclusions

Conclusions

- We have discussed several $f(Q)$ models, highlighting the impact of $G_{\rm eff}$ on cosmological observables and their ability to alleviate the cosmological tensions. We also extended the analysis to $f(T)$ models using additional datasets, showing that the inclusion of a cosmological constant improves the fit to the combined data, yields a higher value of H_0 than ΛCDM, and achieves a goodness of fit slightly better than ΛCDM.
- We have introduced an axion-like model that mimics a dynamical cosmological constant through a tracking regime, providing a fit comparable to that of ΛCDM while addressing the coincidence problem. We have also analysed a 3-form model endowed with a Gaussian potential and tested it against observational data. Finally, we are investigating extensions of the $\Lambda_{\rm s}$CDM model, with the first fits showing promising results.
- Work done in collaboration with H.-W. Chiang, C. G. Boiza, B. Ibarra-Uriondo, J. Ortega del Rio, M. Petronikolou, E. N. Saridakis, I. Ayuso, C.-Y. Chen, X. Y. Chew, K. Dialektopoulos, Y. C. Ong, T. Broadhust and P. Chen

Thank you for your attention !!!